TECHNICAL REPORT No. 37

HIGH RESOLUTION EXPERIMENTS WITH THE ECMWF MODEL: A CASE STUDY

by

Lorenzo Dell'Osso

September 1983

C O N T E N T S

ABSTRACT

The development of mesoscale features in numerical weather forecasts and their evolution as a function of the resolution of the numerical model are studied for the case of Alpine cyclogenesis on the 5th March 1982. The results suggest that the ECMWF model with a reduced grid of about 0.47° (37.0 km at latitude 45°) is capable of improving the forecast and in particular the detail in the surface wind and precipitation. The inadequacy of a coarse mesh analysis for the representation of the mesoscale structure of the fields is discussed and the need for a fine mesh analysis to initialize and verify fine mesh models is stressed.

The use of an 'envelope' type orography to parameterize the effect of mountains on the atmospheric circulation is shown to improve the forecast of the ECMWF model with a 1.875° grid. The height h_e of the 'envelope' orography is computed from the US Navy data set (resolution 1/6°) using the expression $h_e = h + e\sigma$, where h and σ are the mean and standard deviation of the height in the model's grid square and e is a constant. Experimentation with this 'envelope' orography shows that e=1 provides a good parameterization for sub-grid-scale orographic forcing at resolution 1.875°, but e should be decreased with increasing resolution. The separate and combined effect of resolution and orography are examined.

1. INTRODUCTION

Amongst the many requests that a national meteorological service receives, the most pressing is an accurate forecast of wind and precipitation over limited regions. At present, the information that the meteorological service can provide is often not very accurate. Frequently small meteorological features that can cause extensive damage are not reproduced by data assimilation systems and, when they are, their detailed struture is not evident due to the broad scale of the analysis. In addition, even the most sophisticated general circulation models are not able to represent satisfactorily mesoscale structures.

Many modellers have demonstrated the possibility of simulating individual mesoscale circulations, from sea breezes, Estoque (1961), to mountain waves, Klemp and Lilly (1978). Recently, Anthes et al (1982) demonstrated that a variety of subsynoptic systems can be well simulated in a 100 km horizontal resolution model, starting from synoptic-scale data. This corroborates conclusions from earlier studies by Anthes and Keyser (1979) who found that improved forecasts of mesoscale features can be obtained through the use of fine mesh models. The work described in this article lends further support to these conclusions by investigating the separate and combined effect of resolution and orography upon the forecast of low α-mesoscale features.

In particular, it is shown that the ECMWF grid point model described by Burridge and Haseler (1977) and Tiedtke et al (1979) produces more accurate and detailed forecast if the horizontal resolution is increased. To overcome computer memory restrictions when using resolutions of about 0.5°, the limited area version (hereafter referred to as LAM) of the ECMWF grid point model was used; a description of its characteristics is given in the Appendix.

The results described in this article are based on experiments concerning cyclogenesis in the lee of the Alps on 3-5 March 1982 during the Alpex period. The phenomenon of Alpine lee cyclogenesis, its evolution and relation to the Alps has been reviewed by Tibaldi (1980). In this investigation, we are only concerned with cyclogenesis in so far as it can be used to study the effects of resolution in forecasting a mesoscale process that is highly dependent on orographic effects.

In this article there are three main aspects of the investigation which are emphasised. Firstly it is demonstrated that an N192* resolution (37.0 km at latitude 45°) integration can successfully capture the detail of mesoscale features and accurately forecast their behaviour out to 48 hours. The orography used was an 'average' prescription, which was obtained from the US Navy data set - resolution 1/6° - by simple averaging over the model grid square. Secondly, the inadequacy of the present state of the objective analysis in reproducing the detail of mesoscale features is described and the need for a fine mesh analysis to initialize and verify high resolution forecasts emphasized. Finally it is shown that it is possible to obtain a more accurate forecast in a N48 resolution model by using an 'envelope' type orography as a parameterization of sub-grid-scale mountain effects. The 'envelope' orography is obtained from the U.S. Navy data set using the expression $h_e = h + e\sigma$, where h and σ is the mean and standard deviation of the height in the grid square, and e is a constant. This orographic representation already produces an improvement in the medium range forecast of the global model, Wallace et al (1983). Here, its effect on 'local' circulations is examined.

---

*N192 refers to 192 grid points between pole and equator in a regular latitude-longitude grid, i.e. a resolution of 0.46875° or four times the resolution of the operational ECMWF model.

The preliminary results of only one case would appear inadequate for drawing definate conclusions, but recent results from other cases of cyclogenesis in the lee of the Alps, of a vortex south west of Tibet and of a low level jet south east of Tibet, all currently under investigation, support the results presented here.

2. SYNOPTIC EVOLUTION: 3-5 MARCH 1982

This case of Genoa cyclogenesis occurred during the ALPEX period between 3 and 5 March 1982. Figs.1 to 5 show the subjective analysis of the MSLP and of the geopotential height and temperature fields at 500 mb. At 12 GMT 3 March, the 500 mb flow was characterised by a trough approaching the continent; further east there was a ridge followed by a very deep trough over the Mediterranean area which was centred south west of Greece. The corresponding surface pattern had a deep vortex north east of Scotland with the associated front extending from Europe over the Atlantic. In the southern part of the region the area of high pressure, broken by a low centred south of Greece, was invading the Balkans. At 00 GMT 4 March, the deep vortex at 500 mb became cut-off whilst the Atlantic trough approached the European continent. The frontal system at the surface now extended over the continent from Finland to the south of Spain. Further east a region of high pressure was well established in the Balkans and the eastern Mediterrean low started to fill. During the next 12 hours the Atlantic trough continued moving east and by 12 GMT 4 March had reached the western edge of the continent; preceding this trough was a small wave which extended over the western Mediterranean. At the surface the cold front reached the Tyrrenean Sea, whilst the cyclone deepened and spread over the entire region from the Alps to the coast of Tunisia - by this time the low centre was located north west of Corsica and had a central pressure of 1003 mb. The ridge-trough systems in the vicinity of the Pyrenees, Atlas, Appennines and Dinaric Alps show how the shape of this cyclone has been modified by the orography. To the north, the flow, blocked by the Alps, was forced towards central Europe. By the end of the period, 12 GMT 5 March, the trough at 500 mb deepened further and its axis tilted towards the north east.

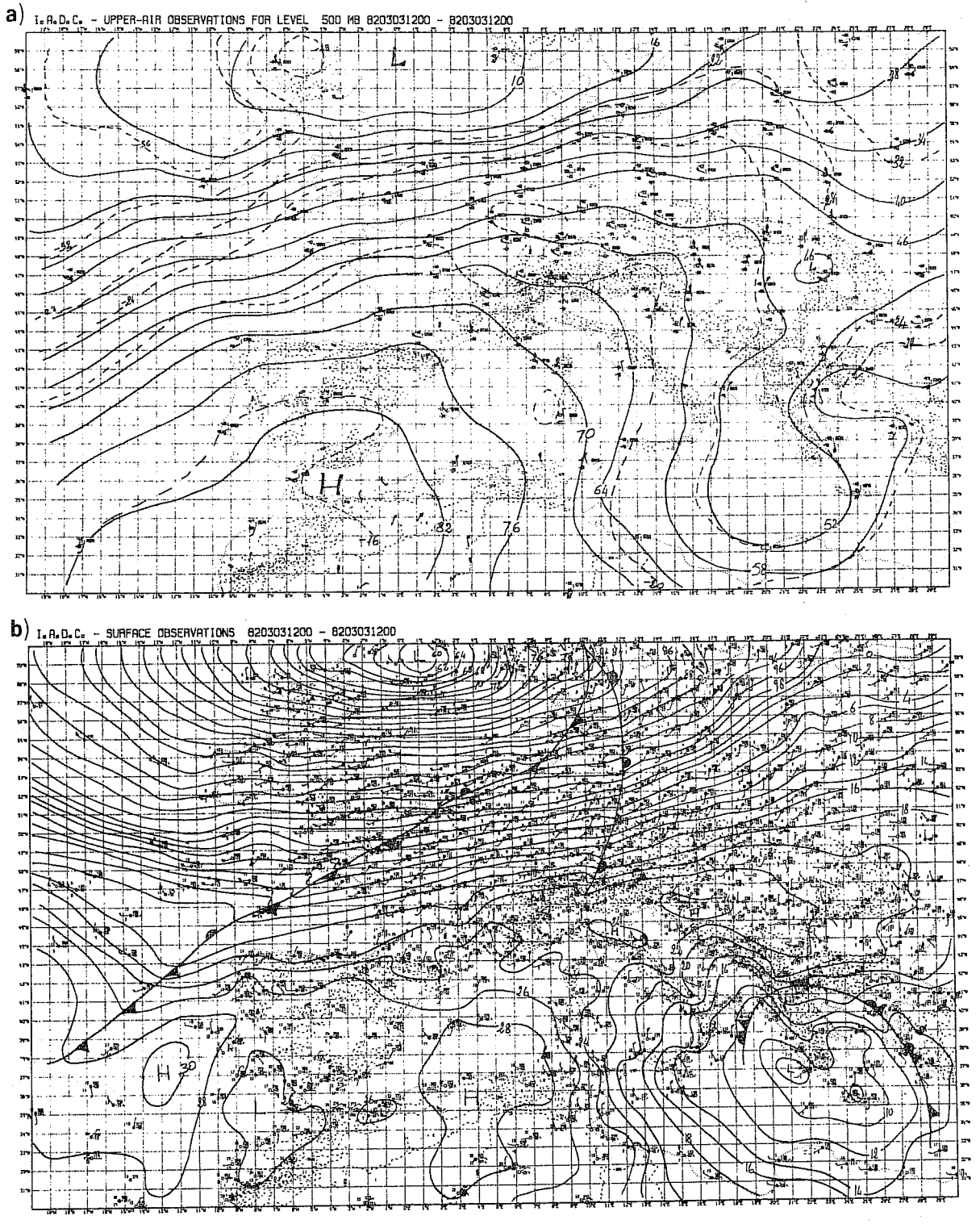

Fig. 1 Subjective analysis for 12 GMT 3 March 1982 of the a) 500 mb geopotential height (isolines every 6 dkm) and temperature (isolines every 4°C), b) MSLP (isolines every 2 mb).

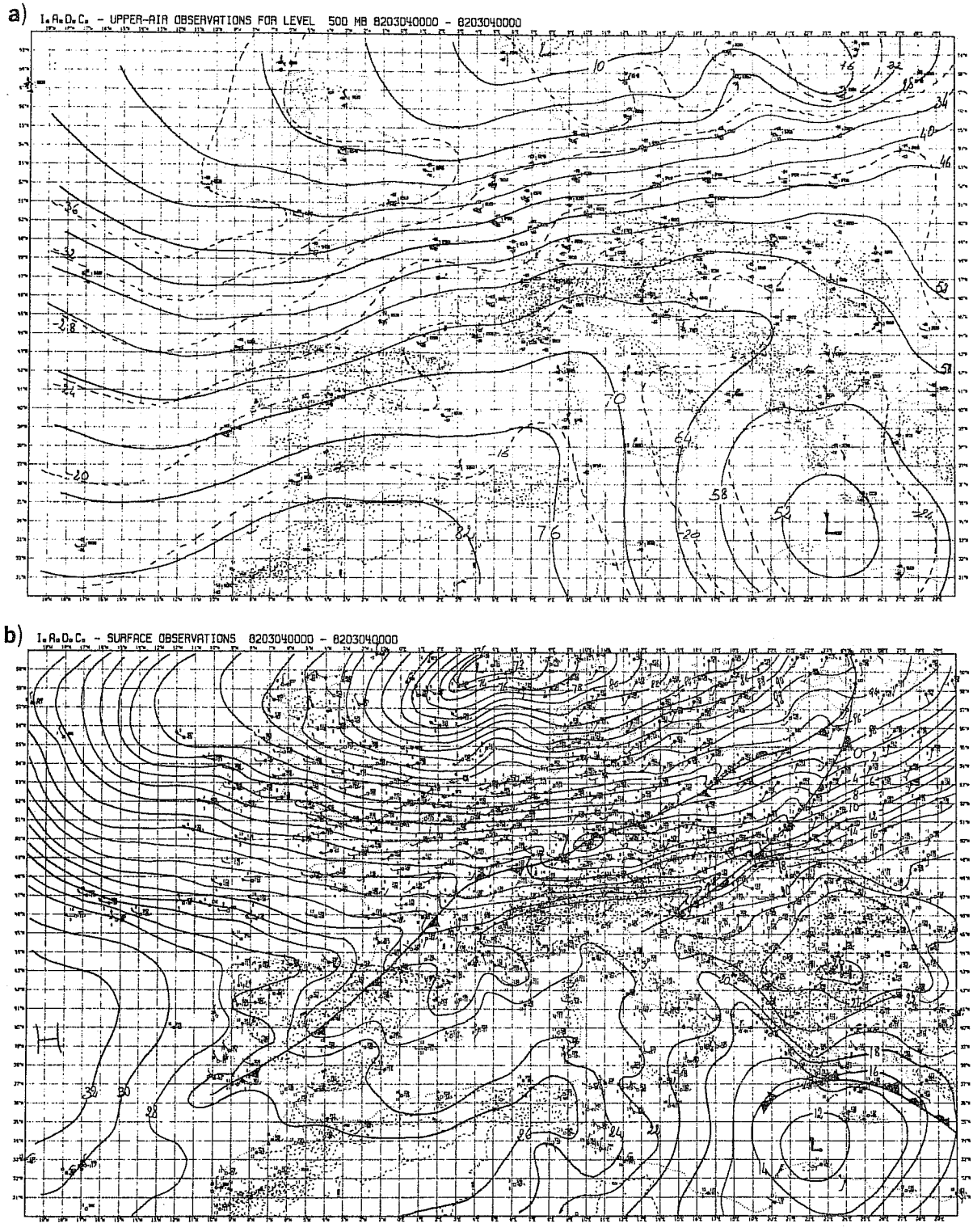

Fig. 2 Same as Fig. 1 for 00 GMT 4 March 1982.

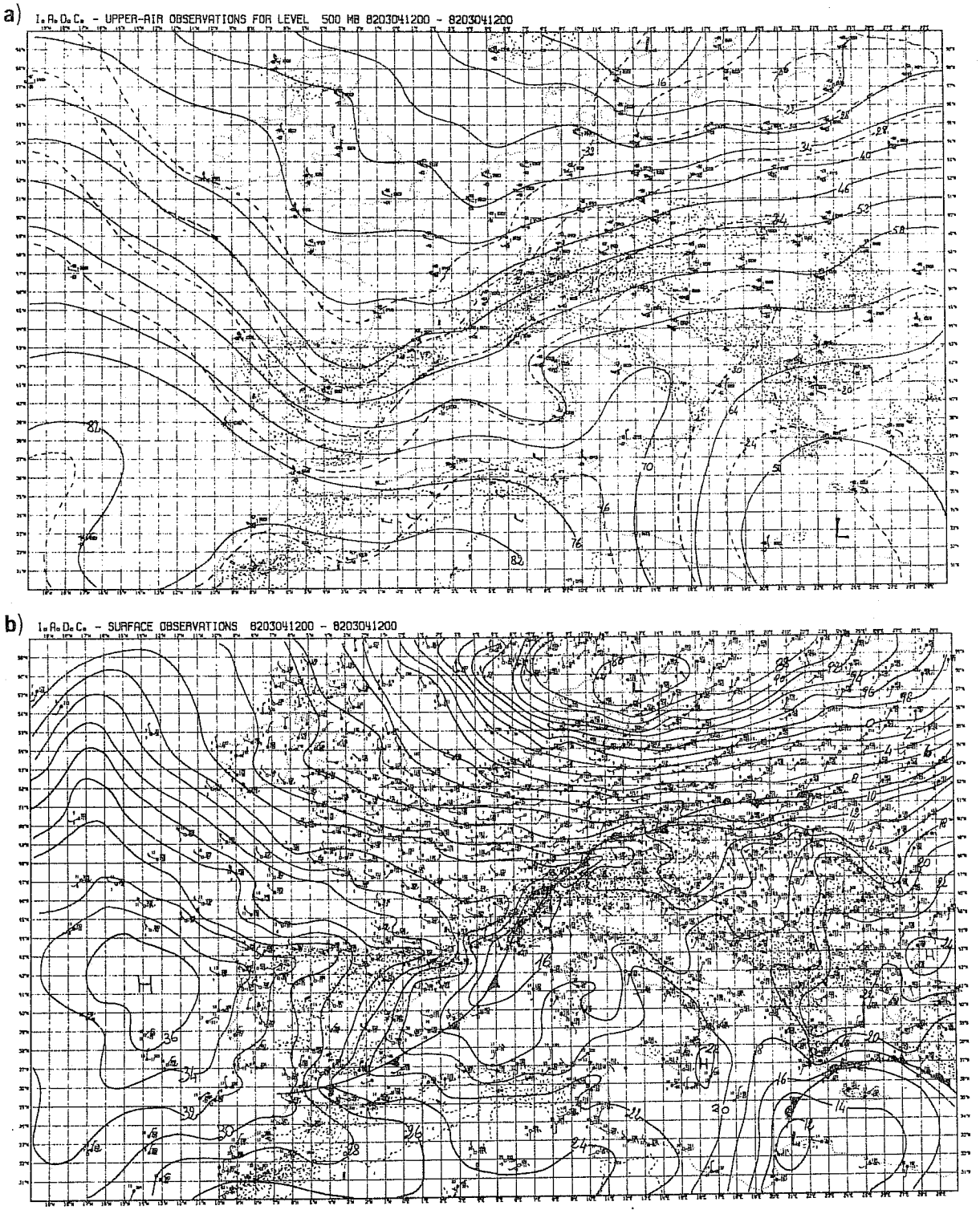

Fig. 3 Same as Fig. 1 for 12 GMT 4 March 1982.

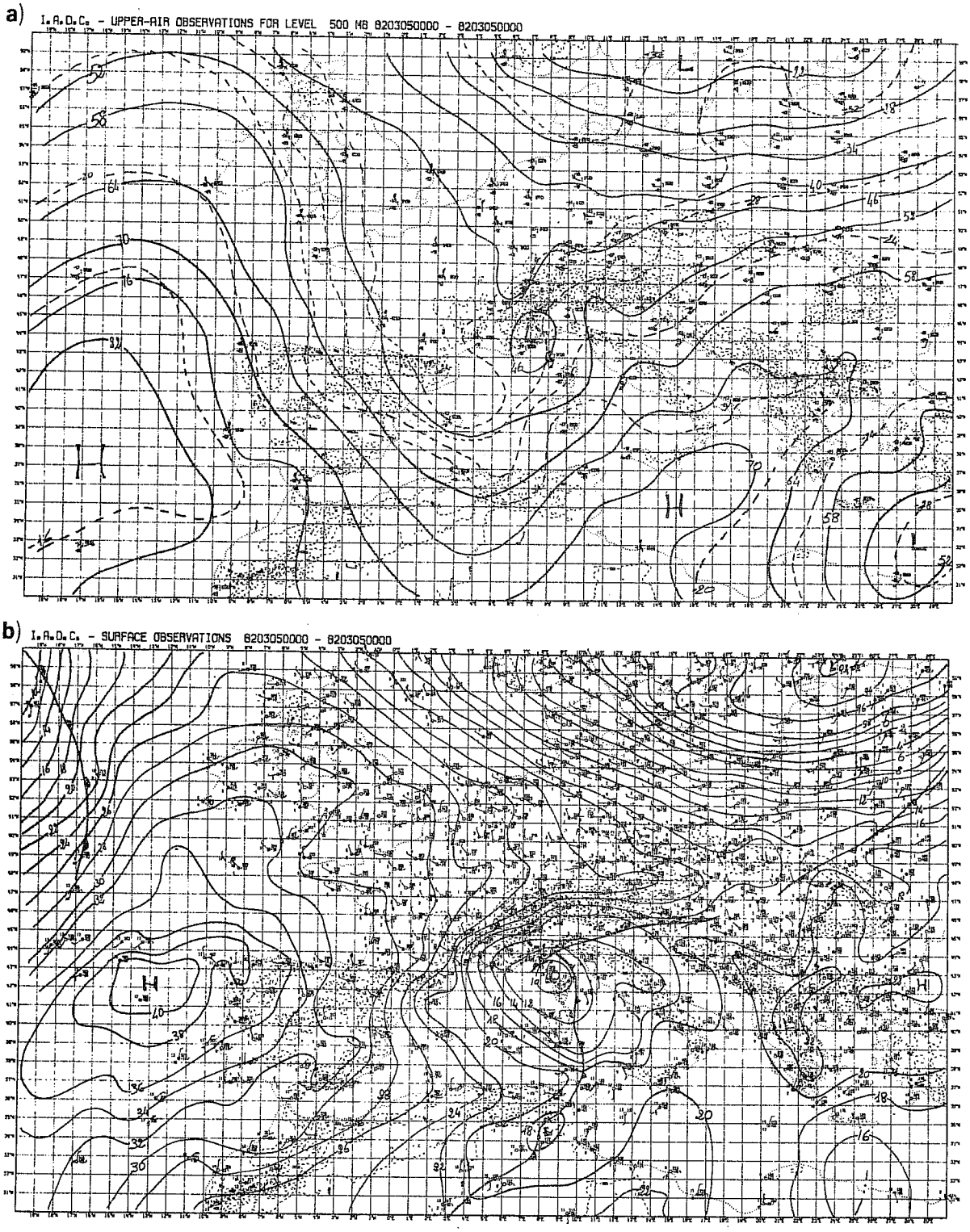

Fig. 4 Same as Fig. 1 for 00 GMT 5 March 1982.

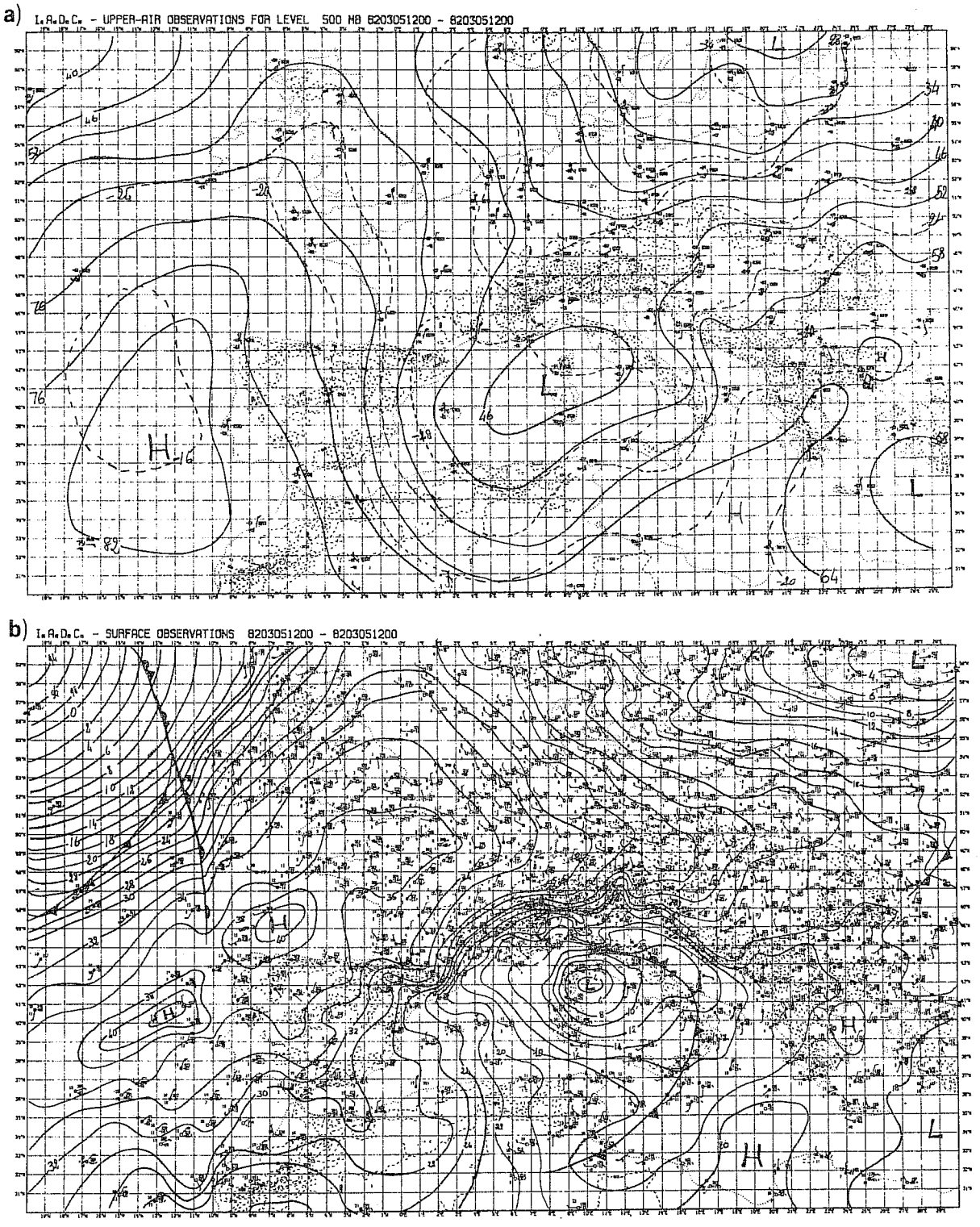

Fig. 5 Same as Fig. 1 for 12 GMT 5 March 1982.

Meanwhile at the surface the cyclone that had travelled to the east of Corsica occluded rapidly and the increased flow along the entire chain of mountain exhibited a set of small scale features, all presumably forced by orography. In the eastern region, the air was able to flow around the eastern edge of the Alps and a small region of high pressure remained near the Peloponnesus. Finally it should be noted that all the usual wind systems of the Mediterranean were present - the Mistral, the Bora and finally the Scirocco that invaded the Adriatic Sea and was subject to the effect of canalisation near the Dinaric Alps.

3. OBJECTIVE AND SUBJECTIVE ANALYSIS

A subjective analysis carried out in the usual way will filter out the short wave features and a great deal of information will be lost. Therefore the subjective analyses for the data dense area over Europe (Figs.1-5) were produced by avoiding all unnecessary "smoothing" and this resulted in the mesoscale features being clearly shown. To do this the analyst used all the observations collected during that particular period and took into account both the large scale flow and the values and tendencies due to local effects. A comparison of this subjective analysis with the objective analysis produced operationally at ECMWF, illustrates that the ECMWF analysis lacks the small scale features of the type that it is hoped to describe in a high resolution forecast model.

Fig. 6a shows the objective analysis (resolution 1.875°) of the 1000 mb geopotential height for 12 GMT 4 March 1982, which is to be compared with the subjective analysis of Fig. 3b. The objective analysis shows a broad area of low pressure instead of the well defined low pressure area with its centre at 44°N 6°E. Note that all the detail found in the subjective analysis concerning the local circulation is absent. The analyses for 12 GMT 5 March (Fig. 7) gives further evidence of the inability of the objective analysis to represent all the small features connected with the orographic effects.

In fact, the Genoa cyclone is in the correct position, but is not deep enough; overall its shape is good but its double structure is missed. Even the ridges and troughs (upwind and in the lee) of the Pyrenees, the Appennines and the Dinaric Alps are missing. That is acceptable when the wave length of these disturbances is less than the size of the mesh of the analysis and the orography is not high or steep enough.

The importance of having a high resolution analysis is twofold; it provides the initial data for high resolution models and the data for their verification. It is certainly possible to obtain a very detailed high resolution forecast even starting from a coarse analysis when the forcing on the lower levels is determined by the orography. However, a coarse analysis can miss small scale baroclinic disturbances and lead to an incorrect high resolution forecast. Furthermore, the effort involved in making a highly refined forecast is not particularly useful if small scale features cannot be verified, and there is a risk of this detail being confused with computational noise. As a consequence it is common to draw conclusions that are biased towards an overly smooth synoptic description of the weather.

4. N48 RESOLUTION FORECAST

Forecasts obtained with the global grid point model and with the limited area model at N48 resolution are presented in this section. Initially the global forecast is assessed against the subjective analysis to reveal where the forecast is inaccurate and what are the likely causes of the errors; then the LAM forecast is assessed against the global forecast to show how faithfully it reproduces the same forecast. Fig.8 shows the geopotential height from the 24 hour global forecast which started at 12 GMT 3 March. At 1000 mb, a region of low pressure over the western Mediterranean area is enclosed within the 16 dkm contour with the actual minimum 6 mb lower (~11 dkm) The blocking of the flow caused by the Alps is certainly not well reproduced by the model. Fig.9a

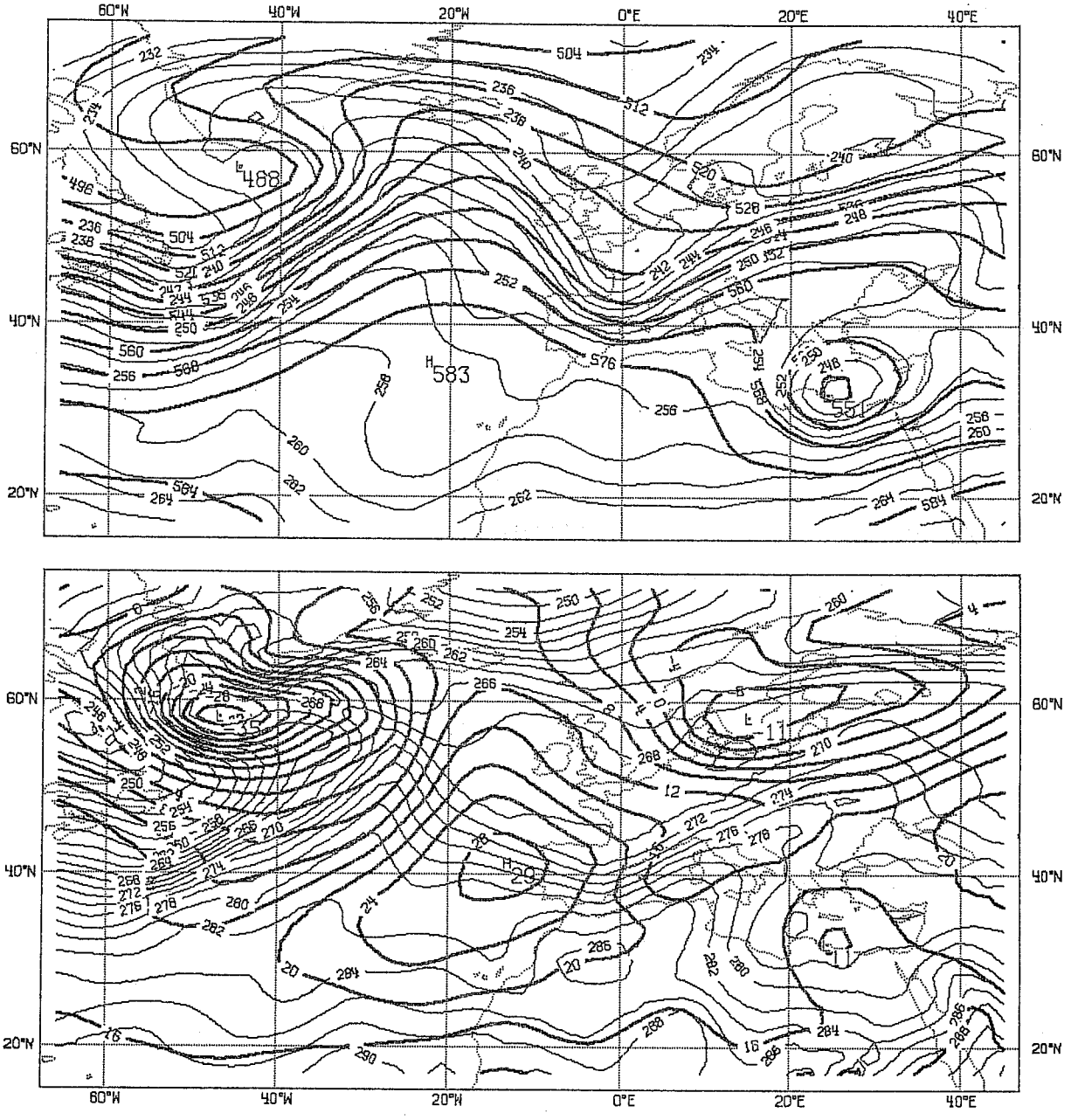

Fig. 6 Objective analysis for 12 GMT 4 March 1982 of the a) 500 mb geopotential height (isolines every 8 dkm) and temperature (isolines every 2K), b) 1000 mb geopotential height (isolines every 4 dkm) and 850 mb temperature (isolines every 2K).

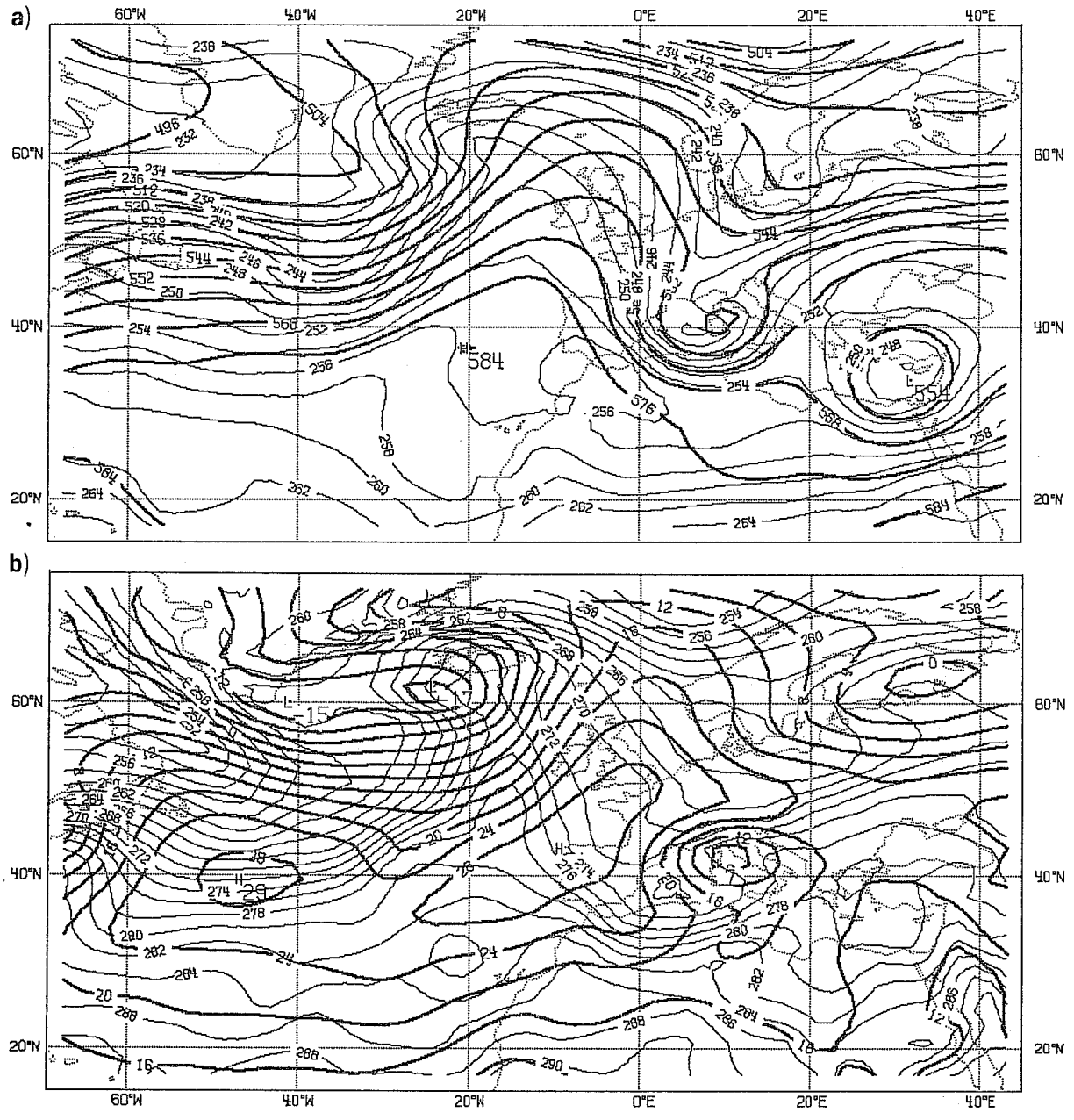

Fig. 7 Objective analysis for 12 GMT 5 March 1982 a) and b) same as Fig. 6.

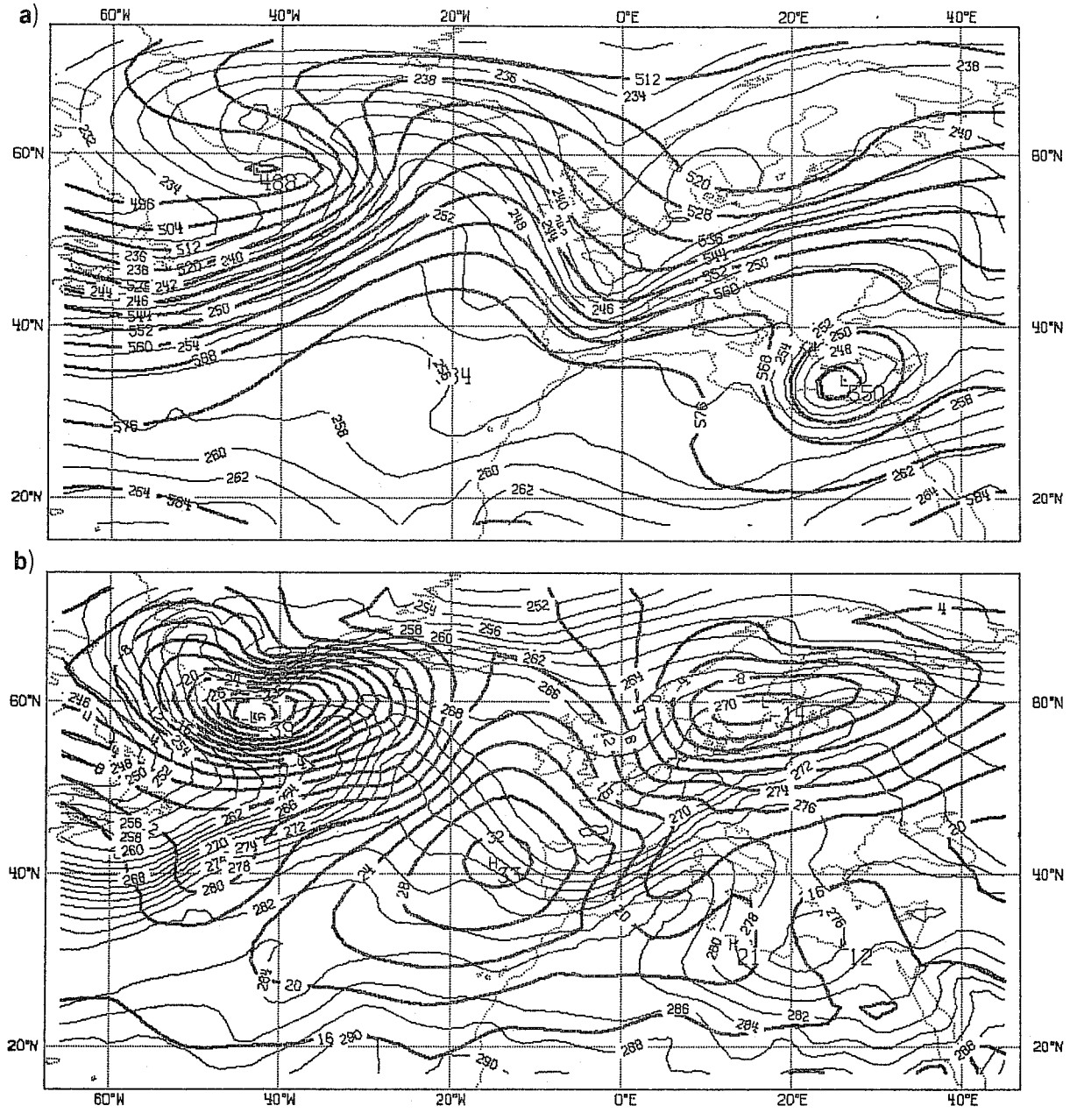

Fig. 8 Maps of the 24 hour forecast ending at 12 GMT 4 March 1982 from the N48 global grid point model, isolines as in Fig. 6.

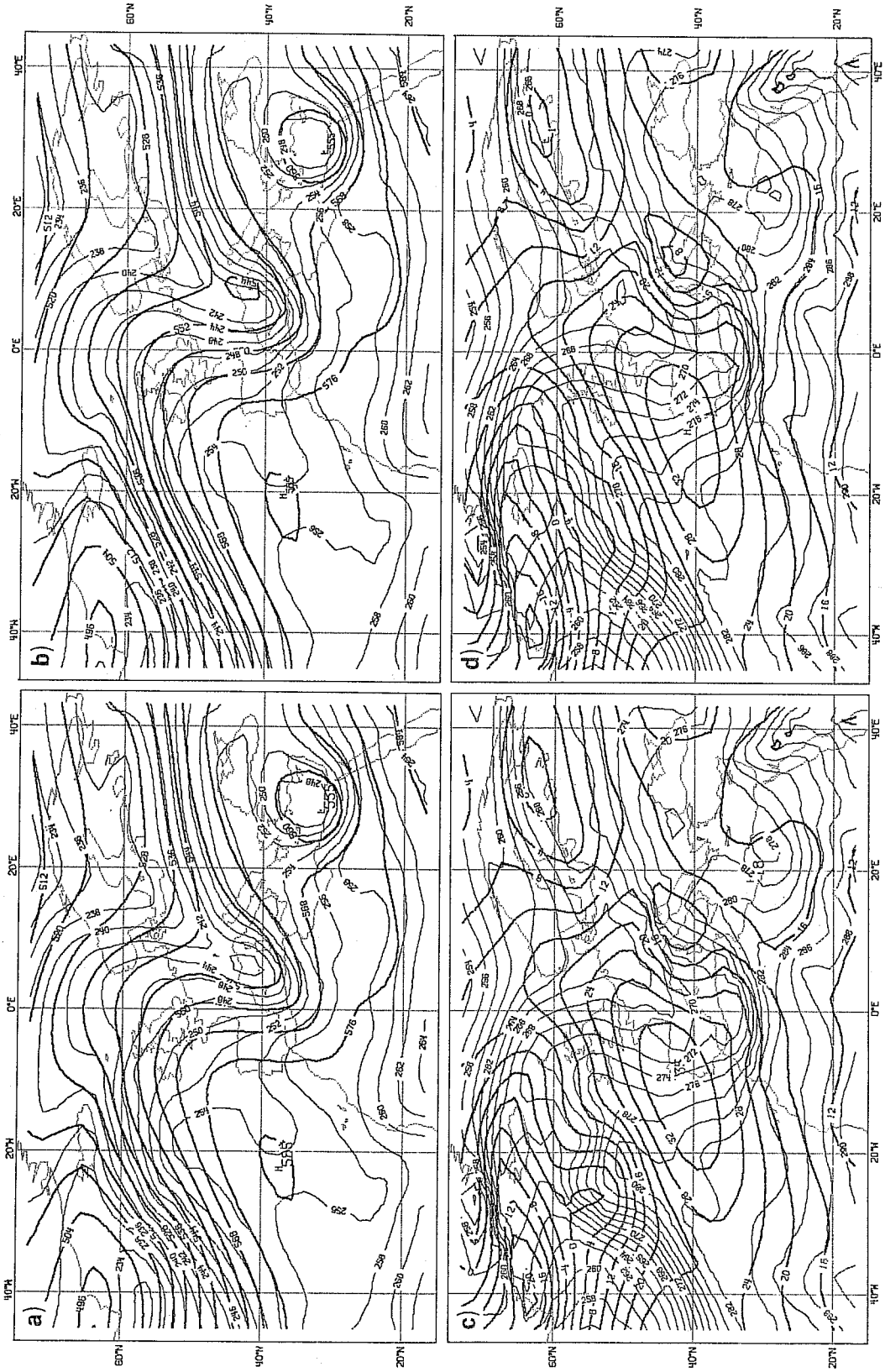

Fig. 9 Maps of the 48 hour forecast ending at 12 GMT 5 March 1982 from the N48 global grid point model (left) and from the N48 limited area model using data from the global forecast to update the boundaries (right). (Isolines as in Fig. 6).

shows the 48 hour, 500 mb forecast from the global model (the verifying chart is given in Fig.5a). The main features of the geopotential height are the trough over the western Mediterranean and the cut-off low over eastern Mediterranean. While the latter is not very different from the analysis (its minimum is south west of what it should be and 1 dkm shallower) the former exhibits a shape that is characteristically different from the one observed. Over Sardinia the analysis shows a cut-off low and a closed contour in the thermal field that are not in the forecast; the model forecast shows only a trough with the axis in north east - south west direction. At the surface the differences are more dramatic (compare Fig.9b and Fig.5b). In the western part of the region, a spurious disturbance forms on the southern flank of an overdeveloped deep vortex that enters the area from the west. This disturbance is accompanied by a spurious secondary ridge in the 850 mb thermal field. The development of the cyclone is forecast, but it is placed too far to the east, not deep enough and stretched in the north east direction. The ridge north east of the Alps does not extend towards east as it should and the thermal field does not show the tongue of warm air associated with the occlusion. The major deficiency of the global forecast is visible in the position, depth and shape of the cyclone.

Figs.9c and d show the 48 hour forecast from the LAM when data obtained from the global forecast is used to update the boundary values. Somehow the model filters the spurious disturbance in the 1000 mb geopotential height produced by the global forecast, Fig.9b. This can be explained if we assume that the LAM is capable of forecasting the fields in the Atlantic region of its internal area in a "correct way". Then global values, affected by errors probably produced in other regions of the globe, enter the relaxation zone and mix with the limited area values, with the result of reducing the amplitude of spurious waves. The cyclone developed by the LAM is slightly deeper than that produced in the global model; however it has a similar shape but is now more

stretched towards the north east: in fact, the ridge north east of the Alps extends eastward even less than in the global forecast. At 500 mb the trough cut-off and its axis is slightly less tilted than in the global forecast, but the position, shape and depth of the eastern Mediterranean cut-off low are identical to that predicted by the global model. It is fair to say that, apart from minor differences, the LAM and the global model behave similarly. This conclusion enables us to assume that all the results obtained from the LAM can be considered representative of what the global model could produce.

In summary we can say that the N48 resolution forecast is not able to forecast accurately the evolution of the cyclone. The reasons for this are connected with the resolution of the model which is insufficient to generate small-scale eddies to reproduce correct α-mesoscale structures and/or represent adequately orographic forcing.

5. N192 RESOLUTION FORECAST

The straightforward use of the global model at resolution N192 would require almost 20 hours of (CRAY-1) computer time for each 24 hour forecast and a considerable reorganisation of the memory; this is beyond the power of the present generation of computers.

Therefore, the LAM (similar in all respects to the global grid point model) was used to carry out a 48 hour forecast at N192 resolution. The initial data is an N48 analysis for 12 GMT 3 March interpolated to the N192 grid with the boundary data being obtained every 12 hours from a 48 hour global forecast and interpolated from the N48 grid to the N192 grid. An 'average' orography is used, see Sect.1 above.

As explained in the Appendix, the initialisation is accomplished by allowing the original orography (the one for N48 interpolated onto the N192 grid) to grow into the N192 orography during the first 12 hours of the forecast.

Figs.10-13 show the geopotential height at 500 and 1000 mb for the 12,24,36 and 48 hour forecasts. It is interesting to compare the 12 hour forecast (Fig.10) with the observed field (Fig.2) to try to detect some possible instability resulting from the orography growth process. Such a comparison reveals that much of what looks like computational noise in the forecast are instead real features present in the observations. For example, note that the ridge which protrudes southwards into the low over the eastern Mediterranean is present in the observations. Examination of the forecast for 12 hours later (compare Fig.11 with Fig.3) shows that it successfully develops the low on the western edge of the Alps. The 36 hour forecast (Fig.12 which verifies with Fig.4) shows a low centred correctly over the Gulf of Genoa and the meandering of the 12 dkm contour represents well the effects of the Apennines; but the low is overdeveloped - its depth being around 1006 mb instead of the observed 1009 mb.

The 48 hour forecast of the 1000 mb geopotential height and wind, Fig.13a and b, can be compared directly with the hand drawn analysis of the MSLP field (Fig.5b) and with the observed wind. This reveals that the double structure of the cyclone is well captured by the forecast with the lowest contour of 4 dkm in good agreement with the observed depth of 1005 mb and the observed secondary low of 1009 mb included in the area contoured by the 8 dkm isopleth in the forecast. The ridge upwind of the Appennines and the trough to the lee are apparent in the 8 dkm isopleth; the ridge and trough related to the Dinaric Alps are found in the 12 dkm contour. Further west, the ridge and trough connected with the orography of the Pyrenees are visible in the deformation of the 20,24 and 28 dkm isopleths. Careful study shows that other features are recognisable in the forecast geopotential.

Now examine the 48 hour forecast of the wind field. The Mistral is present in the forecast with a speed of 25 ms^{-1} whilst the speed observed is 40 ms^{-1}. Following the flow, the wind rotates from northerly to north-westerly; its observed speed is between 20 and 10 ms^{-1}, while the forecast is 20 ms^{-1}. The wind then becomes westerly with a speed of 17 ms^{-1} to the north of Sardinia (an effect of canalization due to the Bocche di Bonifacio is present in the observations) and between 10 and 15 ms^{-1} in the forecast. Reaching the Tyrrenean coast of Italy, the flow becomes south-westerly with the speed decreasing both in the observation and the forecast. The flow then invades the Adriatic sea from the south east (Scirocco) and its speed increases due to the effect of canalization over the Adriatic sea near the Dinaric Alps. The Bora is also present in the forecast near Trieste, where the speed of the wind is forecast between 10 and 15 ms^{-1} and observed as 20 ms^{-1}. A region of very light wind is present in the forecast which is slightly displaced towards the north of that observed. The combined effects of the south-easterly and north-easterly winds over the Adriatic sea is responsible for the high tide in Venice. In fact, the effect of the wind blowing from the south east is to force the water against the closed northern side of the Adriatic. The consequence is the phenomenon of the "acqua alta" (high water) in Venice which can cause considerable flooding. Clearly an accurate forecast of these winds is required as input to the two-dimensional oceanographic models that are used to forecast tide heights in Venice.

In addition to examining the forecasts 1000 mb geopotential and wind, it is important to consider the precipitation. In Fig.14, the comparison between the forecast and observed 12 hr accumulated precipitation suggests that, within the limits of the observed data, the model is able to forecast correctly the spatial distribution of the precipitation but amounts appear to be in excess of 50-100% of those observed. However, a more accurate assessment should be made before reaching any firm conclusion.

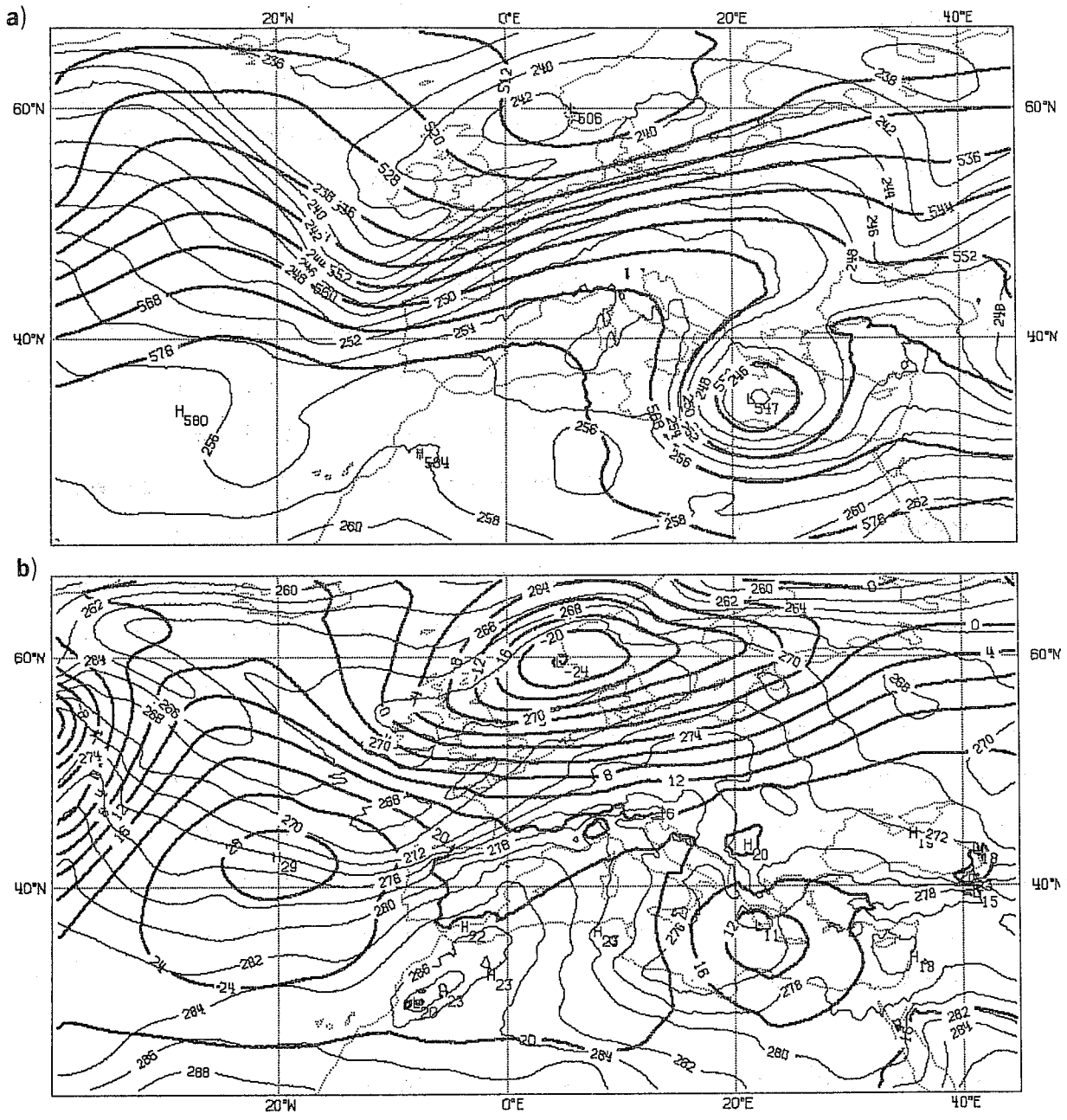

Fig. 10 Maps of the 12 hour limited area model forecast at resolution N192 using average orography and boundary data from global forecast, experiment L. Top and bottom as in Fig. 6.
Verification time 00 GMT 4 March.

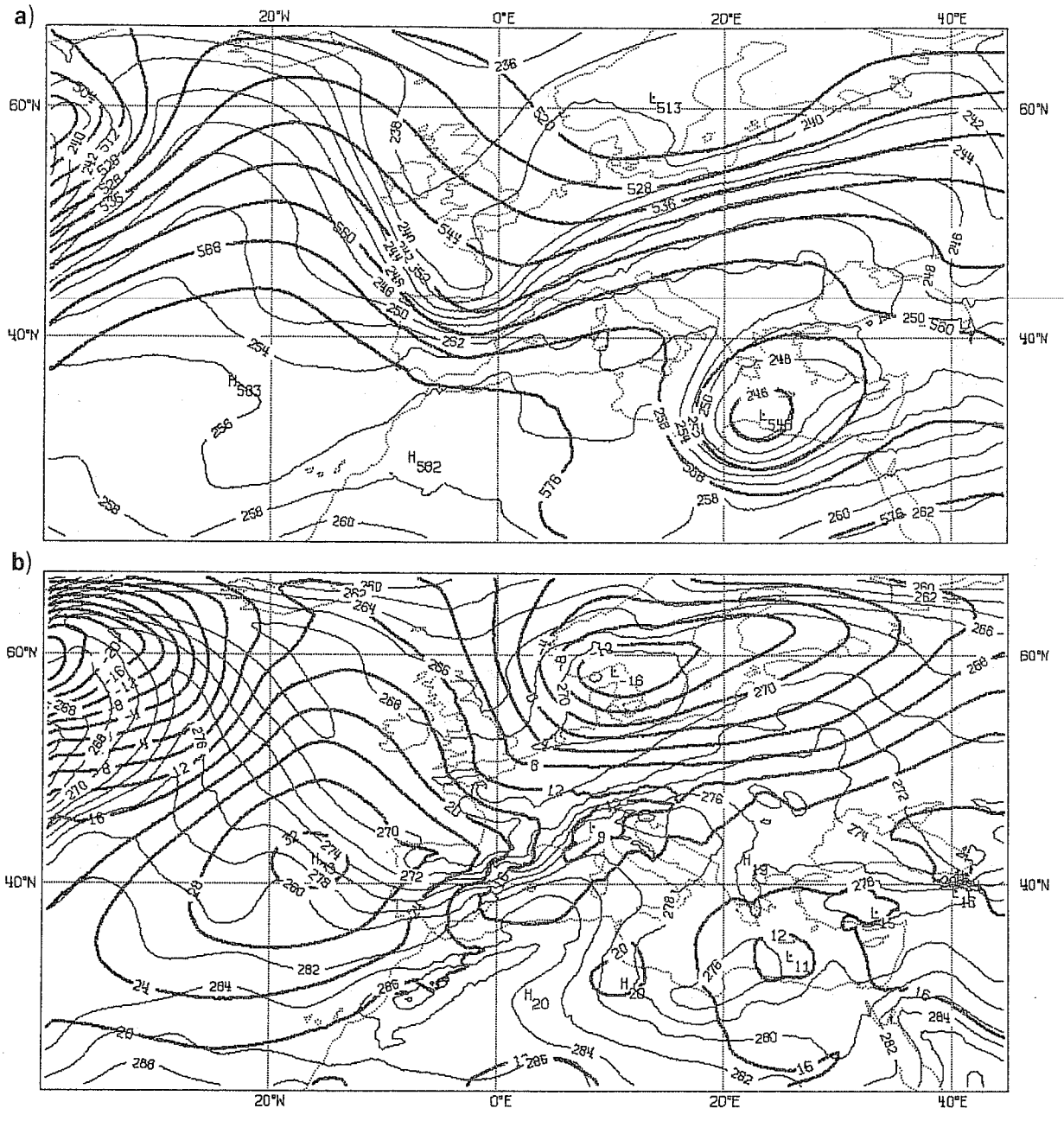

Fig. 11 Same as Fig. 10 for the 24-hour forecast, experiment L. Verification time 12 GMT 4 March.

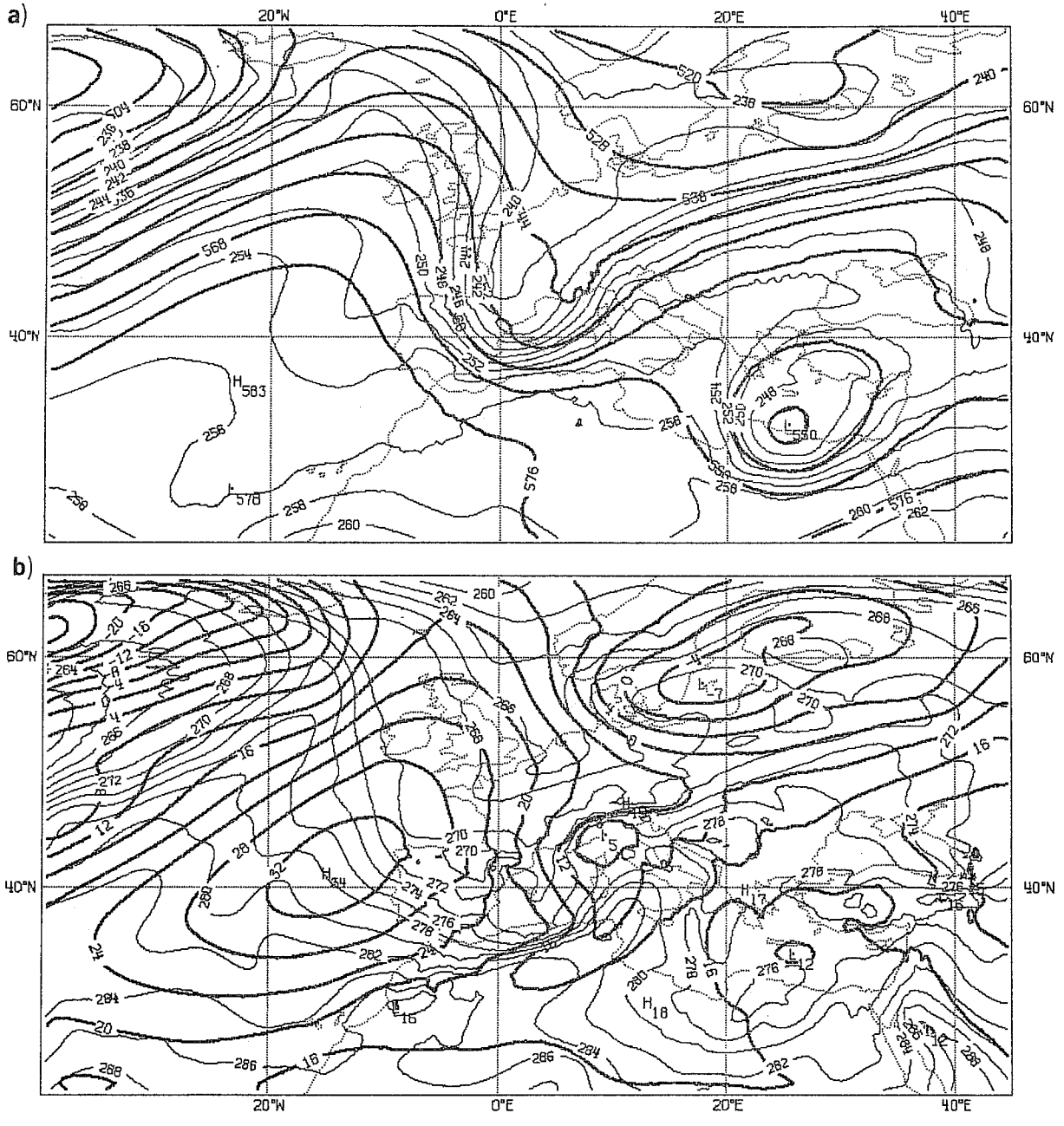

Fig. 12 Same as Fig. 11 for the 36 hour forecast, experiment L. Verification time 00 GMT 5 March.

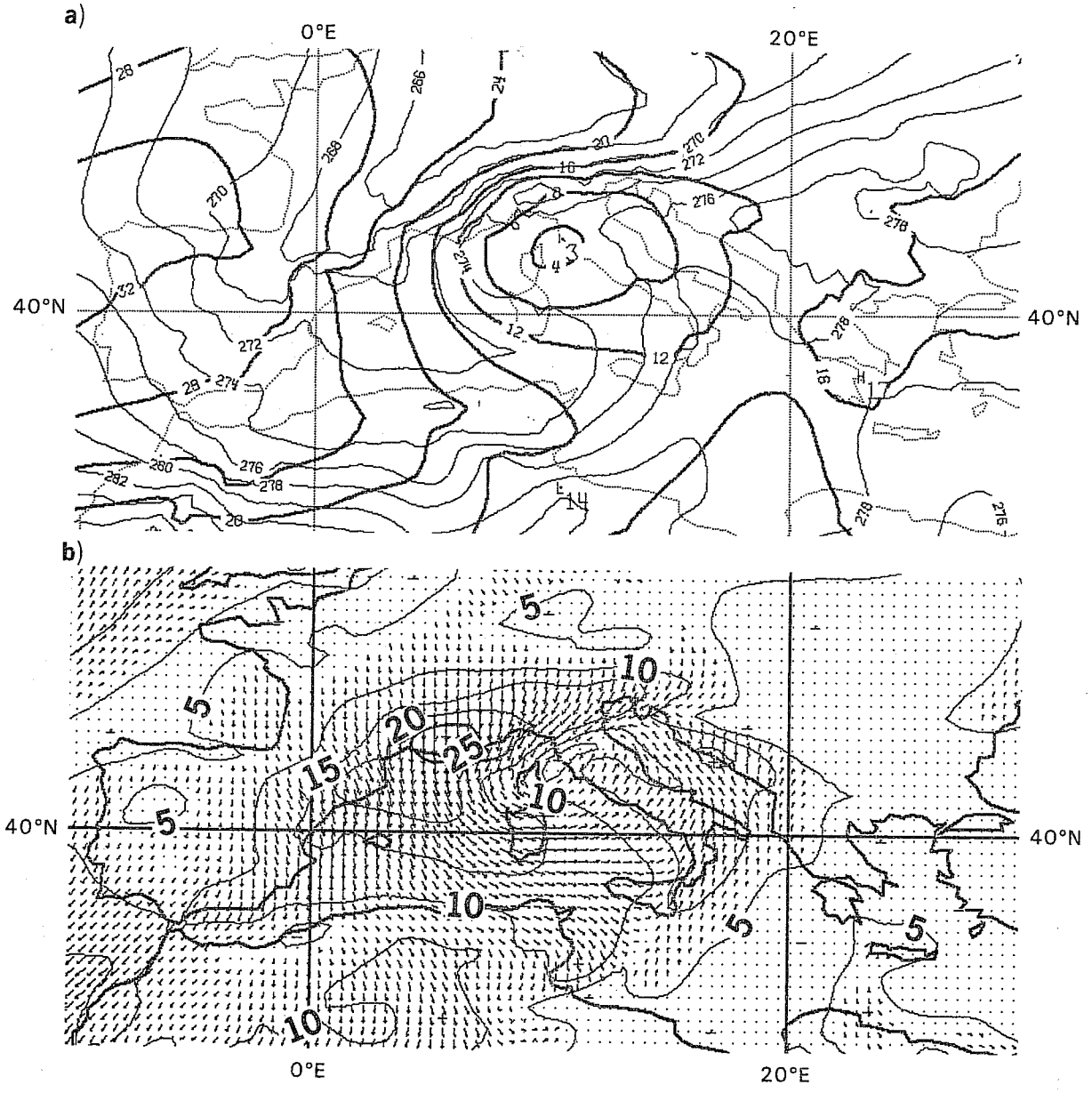

Fig. 13 Maps of the 48 hour limited area model forecast from experiment L for the 1000 mb geopotential height and 850 mb temperature (top), and 1000 mb wind (bottom). (Geopotential and temperature as in Fig. 7, wind isolines every 5 ms $^{-1}$, arrows length proportional to the wind speed).
Verification time 12 GMT 5 March.

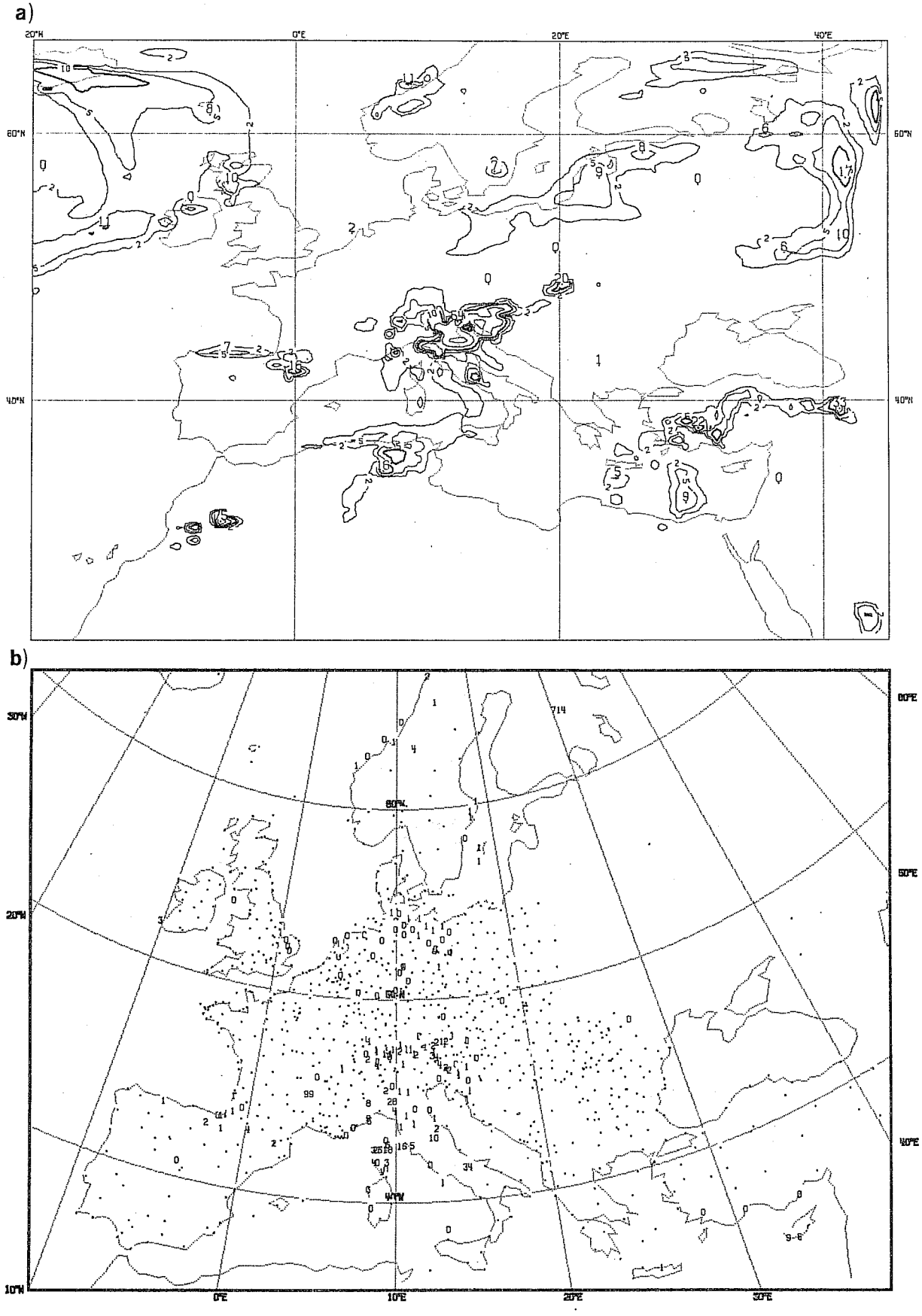

Fig. 14 Maps of the 12 hour accumulated precipitation at 12 GMT 5 March, from a) experiment L and b) observations. (Units in mmH_2O).

6. EFFECTS OF THE HORIZONTAL RESOLUTION

Initially the forecast using the LAM with resolution N48 (1.875°) will be considered - hereafter referred to as experiment A (see Table 1 for a list of experiments). For this, observed data is used to update the boundary values in order to avoid introducing spurious features created in the global forecast that would mask the effects we wish to illustrate.

Fig.15 shows the 48 hour forecast. Comparison with the verifying analysis (Fig.7) shows deficiencies similar to those in the global forecast. For example, at 500 mb a cut-off low forms, but its axis is tilted towards the north east more than in the analysis. At 1000 mb the corresponding cyclone has the correct depth, but is displaced about 3.5° east and 2° north of its true position. Also the forecast cyclone is less stretched and its axis is orientated north-east/south west. Two further forecasts were done to examine the effects of resolution and orography: one at a resolution N96 (.9375°), experiment B, and the other at a resolution N192 (.46875°), experiment C; these are compared with experiment A. To isolate the effect of the increased resolution, it was useful to consider separately the effect of the orography on the atmospheric flow. For this reason, experiments B and C use the interpolated N48 orography which is very smooth. All the maps in this and the next section show the 48 hour forecast starting from 12 GMT 3 March 1982.

The effects of increased resolution on the 1000 mb geopotential height and 850 mb temperature fields are illustrated by comparing experiments B and C (Fig.16). Note that the shape, position and intensity of the cyclone in the lee of the Alps is not well forecast in either of the experiments. We will see that a better representation of the mountains is required. The cyclone is centred too far west and the shape of the cyclone becomes more stretched towards the north-east. Also the flow is not forced around the north-east side of the Alps as it should; this enhances the error found in experiment A

Table 1 Experiments using various resolutions and orographies; A-I used observed data to update the boundary values whereas L used a global forecast.

Experiment	Resolution	Orography
A	N48	'average' at N48
B	N96	interpolated N48 'average'
C	N192	interpolated N48 'average'
D	N48	'1σ envelope' at N48
E	N48	'2σ envelope at N48
F	N96	'1σ envelope' at N96
G	N96	'average' at N96
H	N192	'1σ envelope' at N192
I	N192	'average' at N192
L	N192	'average' at N192

whereby the flow goes around the west side of the Alps which in the model does not present a realistic obstacle - hence all the systems are displaced eastward. Resolution amplifies this deficiency of the orographic representation. In other regions, where the orographic forcing is nonexistent or less crucial, the positive influence of the resolution is apparent. For instance, the simulation of a closed low at 60°N, 40°W is in good agreement with what actually happened but is absent in the experiment A.

The wind field benefits most from the increased resolution. Fig.17 shows the wind field at 1000 mb for the three experiments. To appreciate the different impact of the resolution on the wind field over sea and land, it is convenient to consider the western and eastern sides of the Greenwich meridian separately. In fact, the extensive frontal system over the Atlantic is almost undisturbed by any land effect. Going through experiments A to C, the sharpening of the front is evident: this feature, originally broad and ill-defined, becomes smaller. It is worth noticing the 'kink' in the 10 and 15 ms^{-1} isopleths near the British Isles in Fig.17: the wind field is affected by the presence of the land that, in experiment C, is represented by a number of points ten times larger than in experiment A, where this deformation is absent. The land-sea indicator of Fig.18 show how the coarse definition of the land area in the N48 version is refined in the N96 and N192 resolutions. The superiority of the high resolution forecast is demonstrated dramatically in the Mediterranean region; even with a poor orography the model with the N192 resolution is able to produce the strength and direction of winds such as the Mistral and Bora. Obviously, with the centre of the low being displaced eastward, the wind over the Adriatic sea is not the Scirocco but a southerly wind.

When examining the vertical velocity at 500 mb and 700 mb in experiment A,B, and C (Fig.19), the effect of the resolution on the horizontal gradient of the vertical velocity is evident in the large frontal system over the Atlantic. Not only does the maxima of the vertical wind increase, but the area occupied by the frontal system shrinks dramatically from experiment A to C. Frontal systems over land behave in a similar way; the frontal activity becomes better defined and the occlusion is increasingly pronounced in the Alpine region. The shape of the very strong horizontal gradient of the vertical wind at 700 mb gives a clear indication of the effect of the inaccurate representation of the orography.

The accumulated precipitation in the previous 12 hr, Fig.20, clearly shows the benefits brought about in the precipitation forecast by improved resolution. The frontal systems are better defined in B and C than in A, but in addition the resolution is capable of producing precipitation in areas where it was not forecast in experiment A. In experiment C the Atlantic region exhibits a great wealth of detail and activity not seen in experiment A. However in the eastern Mediterranean region, there are patches of convective precipitation that may be spurious since they do not have their counter-part in the observations.

The effects of increased resolution can be summarised by considering the cross-section A-A marked in Fig.16. Fig.21 (top) shows the increasing sharpness of the horizontal wind gradient as the resolution increases from N48 to N192: at low levels around latitude 43°N, where there is a sharp increase of vertical velocity and at upper and low levels around latitude 47-49N, where the surface pressure deepens considerably. Fig.21 (middle) show the intensification of the vertical velocity from experiment A to C, while Fig.21 (bottom) show the effect of the resolution in creating cloud with a greatly increased internal structure and vertical extent (as in the cloud in the region between 48°N and 49°N).

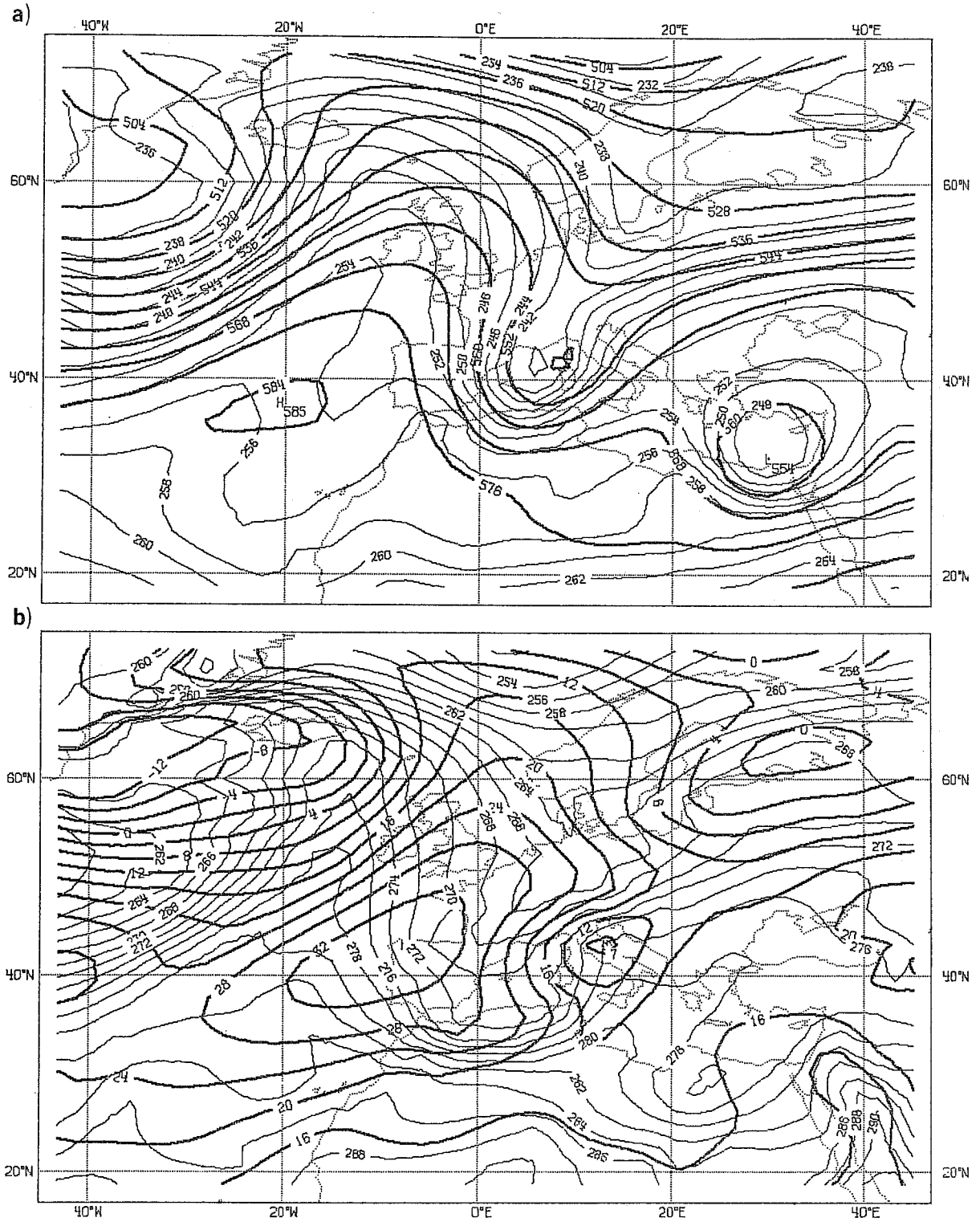

Fig. 15 Maps of the 48 hour forecast from the N48 limited area model using data from the analysis to update the boundaries, experiment A.
a) and b) as in Fig. 7.
Verification time 12 GMT 5 March.

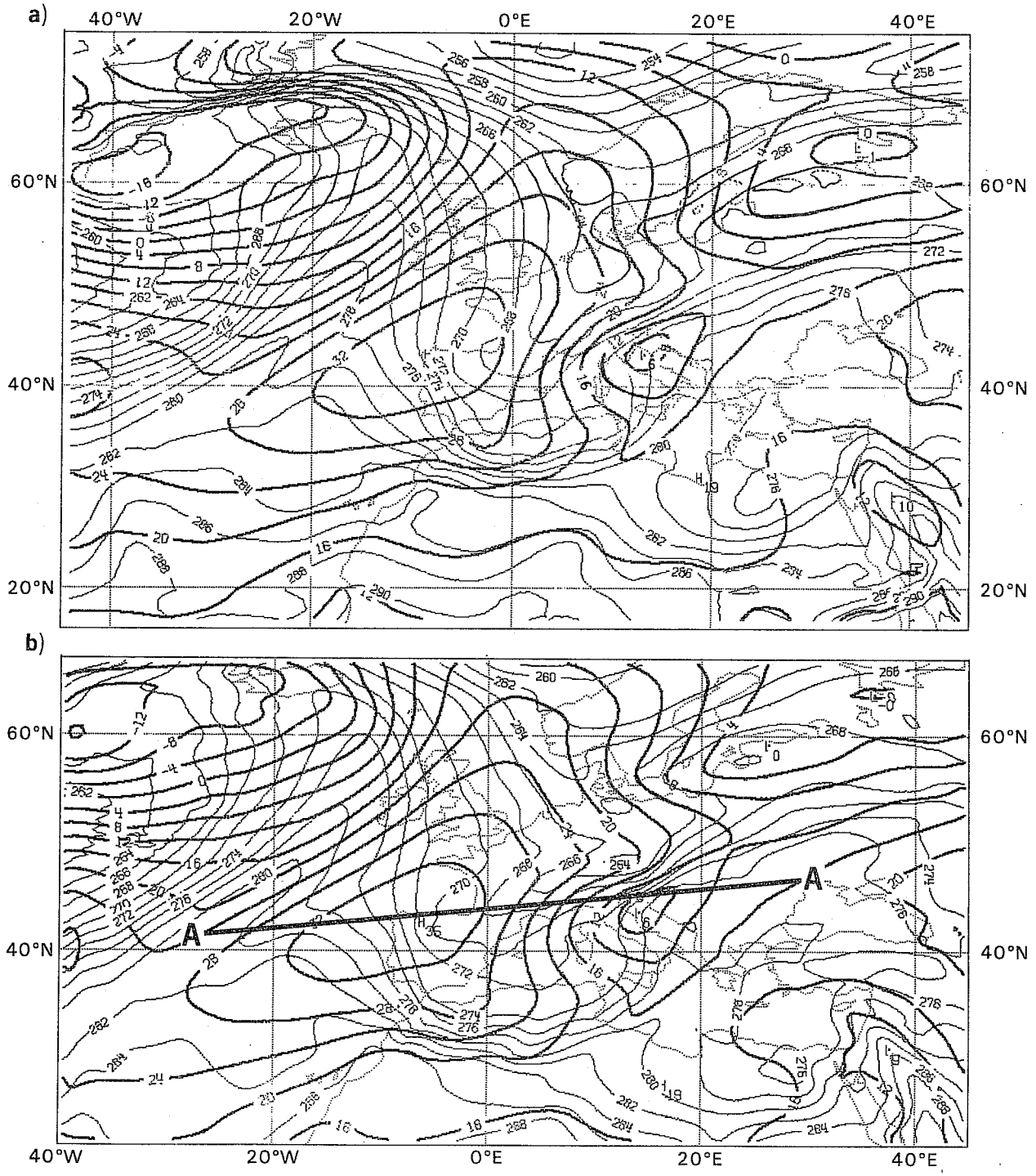

Fig. 16 Maps of the 48 hour limited area model forecast for the 1000 mb geopotential height and 850 mb temperature, at resolution a) N96, experiment B, b) N192, experiment C. (Units and contours as in b) of Fig. 7).

Verification time 12 GMT 5 March.

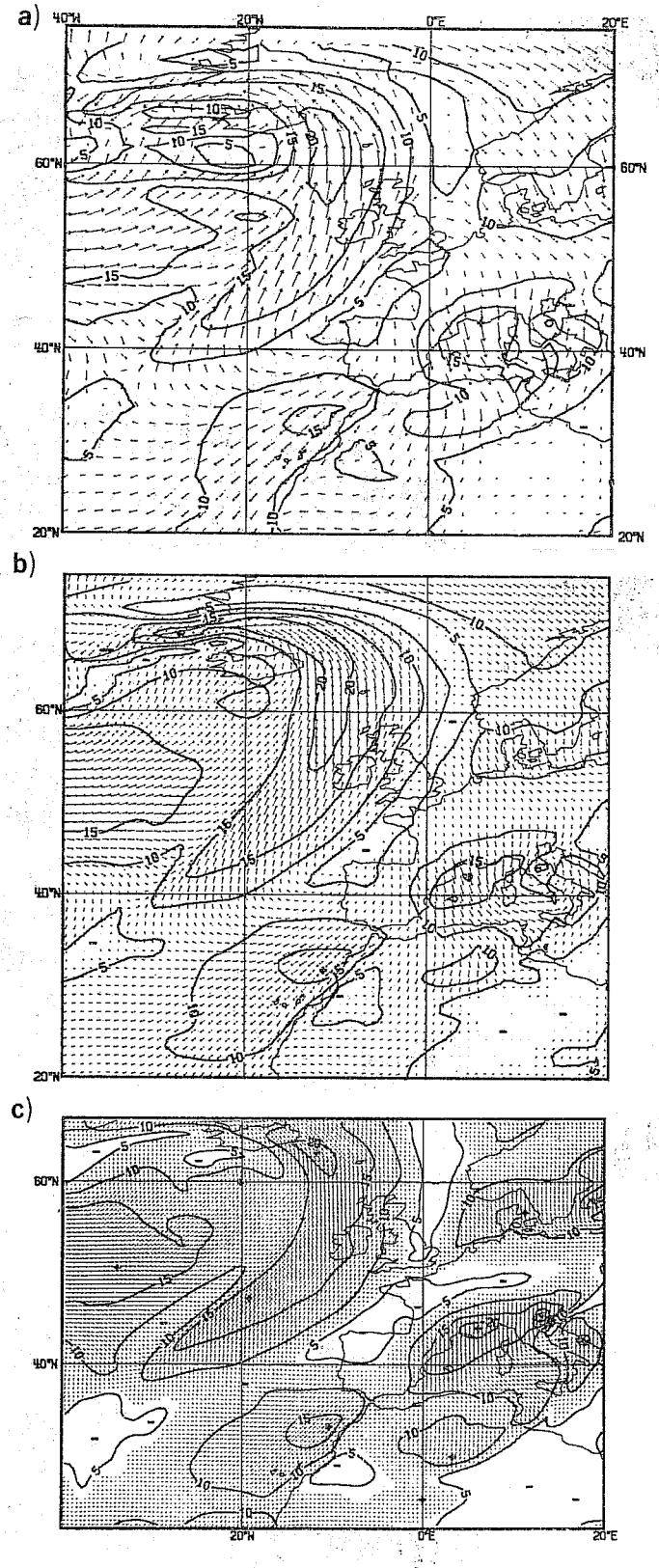

Fig. 17 Maps of the 48 hour forecast for the 1000 mb wind field from the limited area model at resolution a) N48, experiment A, b)N96, experiment B, c) N192, experiment C. The orography is the interpolated N48. (Isolines every 5 ms^{-1}, arrows length proportional to the wind speed).

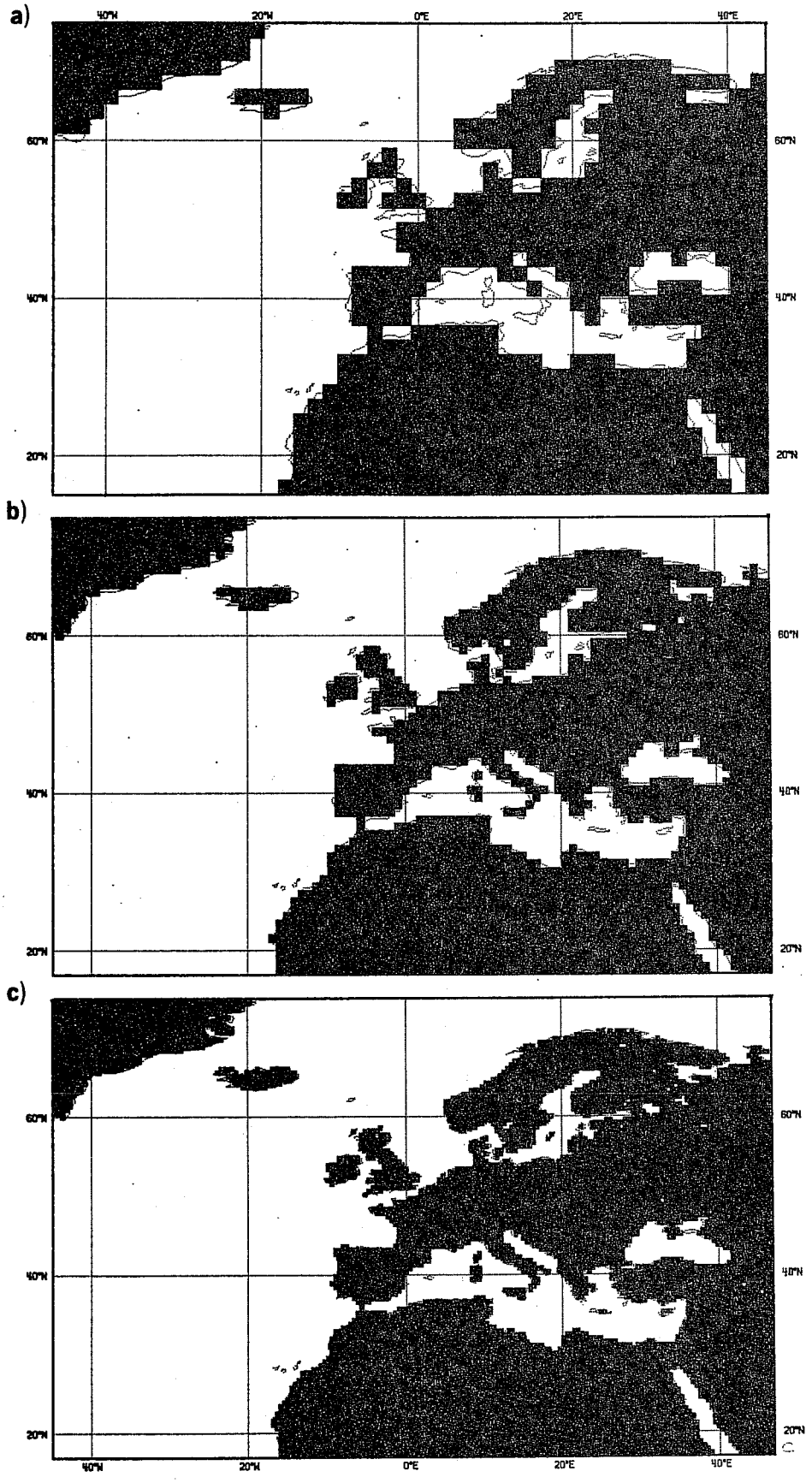

Fig. 18 Maps of the land-sea mask at resolution a) N48, b) N96, c) N192.

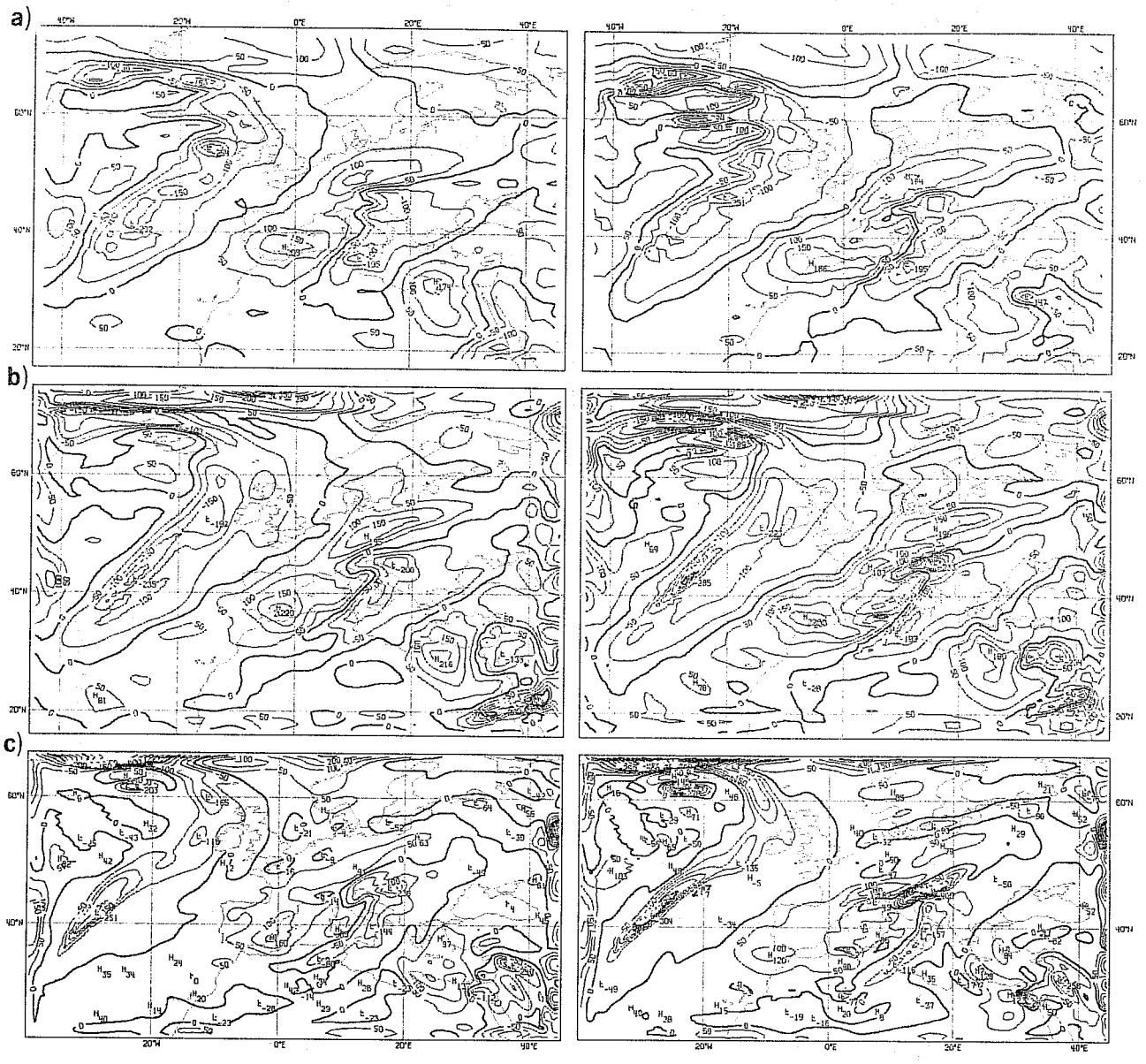

Fig. 19 Maps of the vertical wind at 500 mb (left) and at 700 mb right), from the limited area forecast at resolution a) N48, b) N96, c) N192, (experiments A,B,C respectively). (Units: 10-3 Pa s-1).

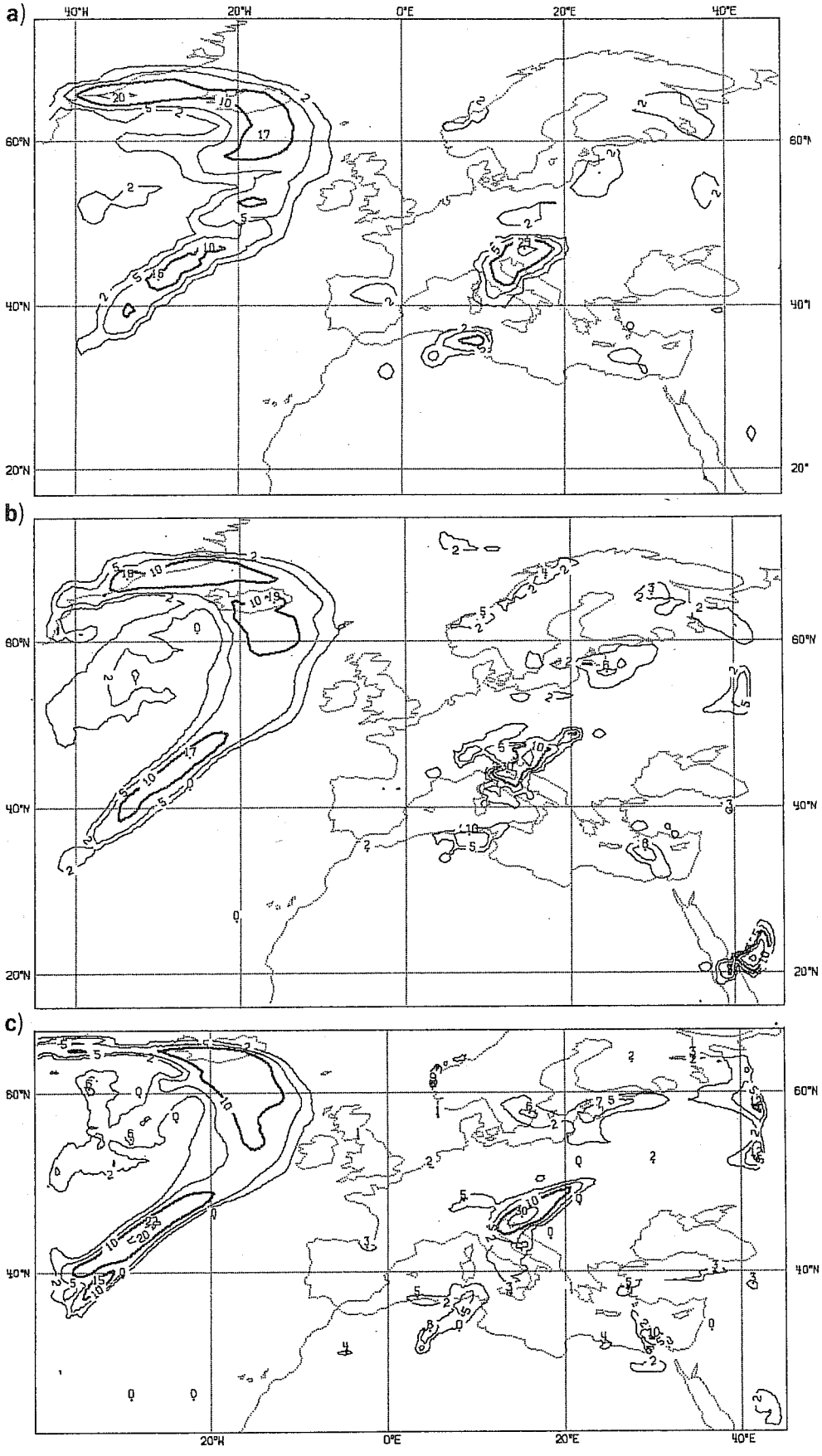

Fig. 20 12 hour accumulated precipitation from the 48 hour limited area model forecast at resolution a) N48, b) N96, c) N192.

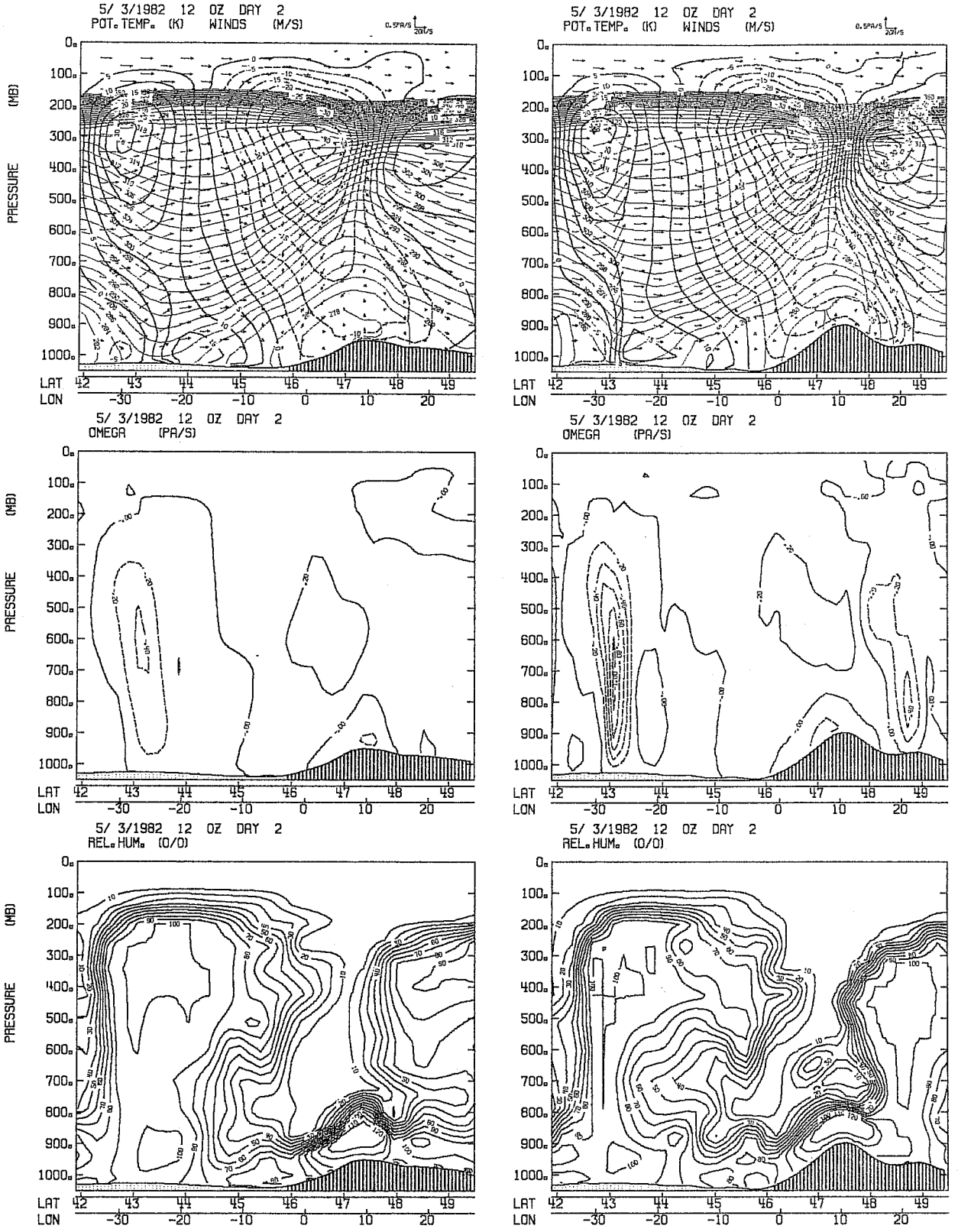

Fig. 21 Vertical cross section along line A-A shown in Fig. 16 of the 48 hour limited area forecast at N48 (left) and N192 (right) resolution. Top: thin lines are isentropes (isolines every 2K), thick lines are isotachs of the component of the wind perpendicular to the plane of cross section (in ms^{-1}, positive into the plane) arrows are proportional to wind speed parallel to the plane of cross section. Middle: omega in Pa/s. Bottom: relative humidity in %.

A consequence of increasing the horizontal resolution in a numerical model is the ability to resolve smaller eddies and hence the fine structure of the meteorological systems is better defined. The increased resolution can affect considerably the wind and, consequently, the forecast of the precipitation is improved both in its location and quantity. Indeed, a frontal system is a large scale phenomena when viewed along its length, but is of mesoscale nature across the front; however, the inner structure of the convective phenomena is undoubtedly of a smaller scale. Therefore, if the model is able to capture the small scale activity in more detail, it is reasonable to expect that a better forecast would result.

Unfortunately the state of the art of the objective analysis for fine scale models and verification is in its infancy. Therefore the following resolution experiments use analysed data interpolated from the N48 ECMWF objective analysis. However, parameters such as albedo, roughness and land-sea indicators, should be consistent with the resolution as should the orography. The orography, in particular, has to be prescribed with the detail, steepness and height appropriate to the relevant resolution.

7. HORIZONTAL RESOLUTION AND OROGRAPHY

In Sect.6, the resolution was increased whilst keeping a very smooth orography. However, from those experiments it appears that the orography must be chosen with the same detail as the resolution of the model. In Sect.4 and 5 we saw that 'average' orographies are good at N192 resolutions but inadequate for the lower resolutions. The detail and steepness of the mountains at N192 is close to the detail and steepness of the US Navy orography and the model is capable of using this detail. The 'average' orography at N48 seems to be too smooth to create an obstacle to the flow comparable to the effect of the actual mountains. Consequently, there is a need to find an orographic representation at a N48 resolution which is able to influence the

flow in a way similar to that attained in N192 model with an average orography. In this section we examine the performance of the 'average' and the 'envelope' orography at three resolutions - N48, N96 and N192.

As described in Sect.1 the 'envelope' orography is computed by using the formula $h_e = h + e\sigma$. In the following experiments, the orographies obtained with e=1 ('1σ envelope') and e = 2 ('2σ envelope') are used. The representation of the 'average', ' 1σ envelope' and '2σ envelope' orography at resolution N48 are given in Fig.22.

In Fig.23, the 1000 mb and 500 mb geopotential height from the N48 forecast with '1σ envelope' orography (experiment D) is compared with that one obtained using the '2σ envelope', (experiment E). The most obvious difference between the two 1000 mb fields is the position of the cyclone. In D, it is located over the west coast of Italy, while in E it is displaced 2° west of Corsica. Fig.22 suggests that the orography is responsible for the displacement. For experiment E, all the Alpine mountains are higher than in D; in particular they extend west, obstructing the Rhone valley and forcing the flow too far west. Due to the steepness and height of the mountains on the east side of the Alps in experiment E, the flow is forced too far east - the 24 dkm isopleth goes beyond 20°E, while according to the observations it should stop around 10°E.

Fig.24 shows successive zonal cross section of the region from the Massif Central to the sea. Note how at 45°N the flow is obstructed in experiment E, while in D there is a low level northerly wind component with a maximum of 25 ms^{-1}; at 44°N, the maximum at low level in experiment E is at least 2° further west than in D. Finally at 43°N, the flow in E is not only displaced at least 2° west, but its speed is 5 ms^{-1} greater than in D. It seems clear that, while the presence of Alps and Pyrenees is important for the formation of the Genoa cyclone (Trevisan, 1976), the position of it is certainly

dependent on the presence of the gap between the two chains of mountains. The 500 mb geopotential height for these two experiments is shown in Fig.23a and c and, when compared with the objective analysis, shows that only in experiment E was a cut-off low obtained over the region of the cyclonic development. The axis of the trough is more tilted than in the analysis, and the round shape of the analysed trough is better modelled in experiment E; but the ridge west of it is far too north and east of the retrogressed trough. All these features that were already apparent in experiment A are exaggerated by the over-steep and high mountains of experiment E. The '2σ envelope' orography is probably able to influence correctly the standing waves as in the experiments carried out with the global model by Wallace et al (1983). But it is certainly not suitable for the representation of orographic details that can affect the local weather. Hence the choice of the '1σ envelope' orography which was used in the next experiments.

In Figs.25 a and b, the '1σ envelope' orography is compared with the 'average' orography at N96 resolution. The 'envelope' orography is clearly steeper and higher than the 'average' and this is reflected in the comparison between experiment F, which used the 'envelope' orography and experiment G with the 'average' version (Fig.26). As already seen for the N48 resolution, the envelope orography is able to determine the shape and position of the cyclone considerbly more accurately than the average orography. At 500 mb, the trough of the geopotential height in experiment F shows a round shape similar to the objective analysis. Obviously the lack of resolution does not permit the detail that can be seen in the N192 resolution experiments.

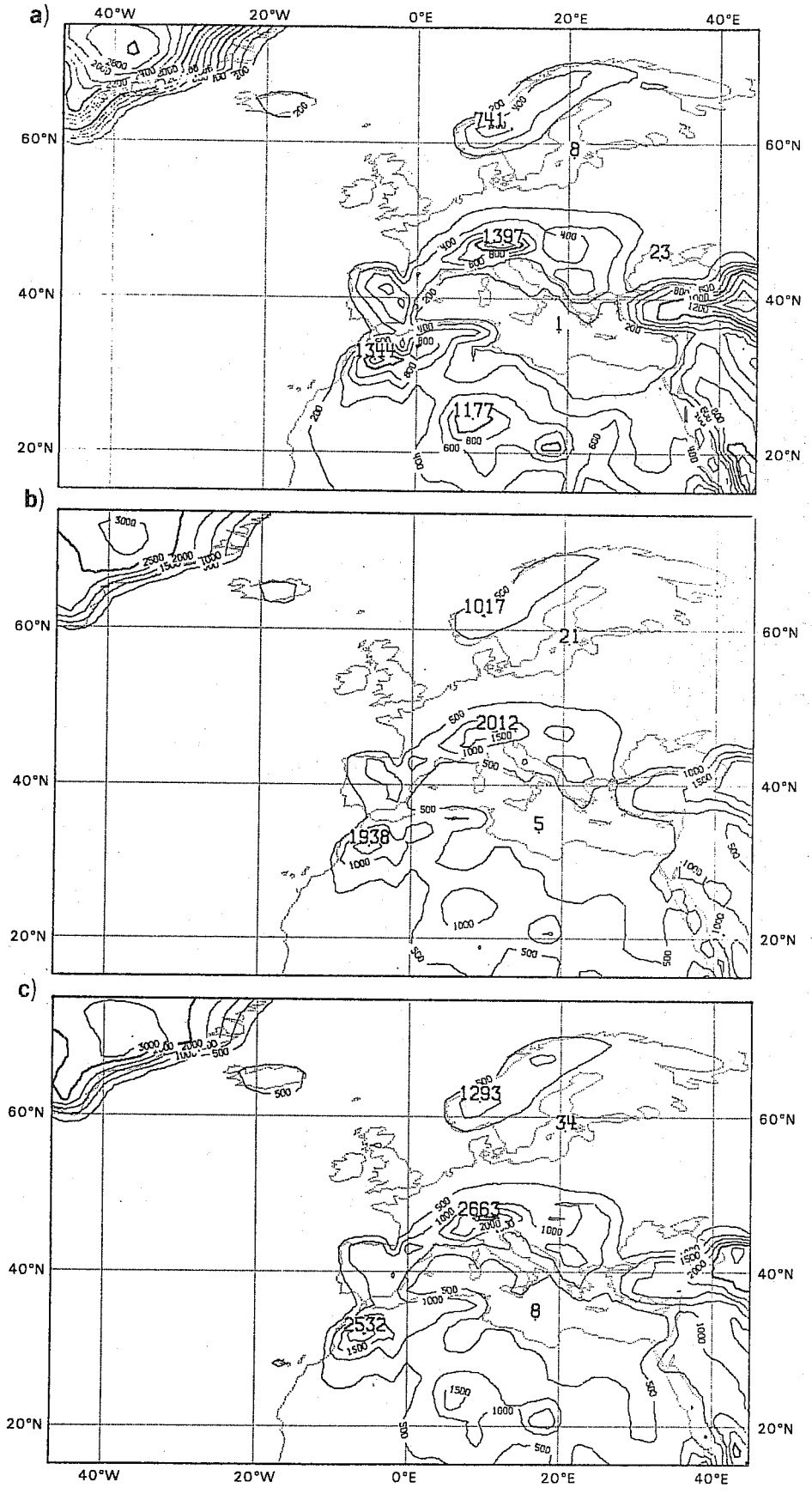

Fig. 22 Maps of the orography at N48 resolution: a) average orography, b) envelope orography with one variance, c) envelope orography with two variances. (Units in meters).

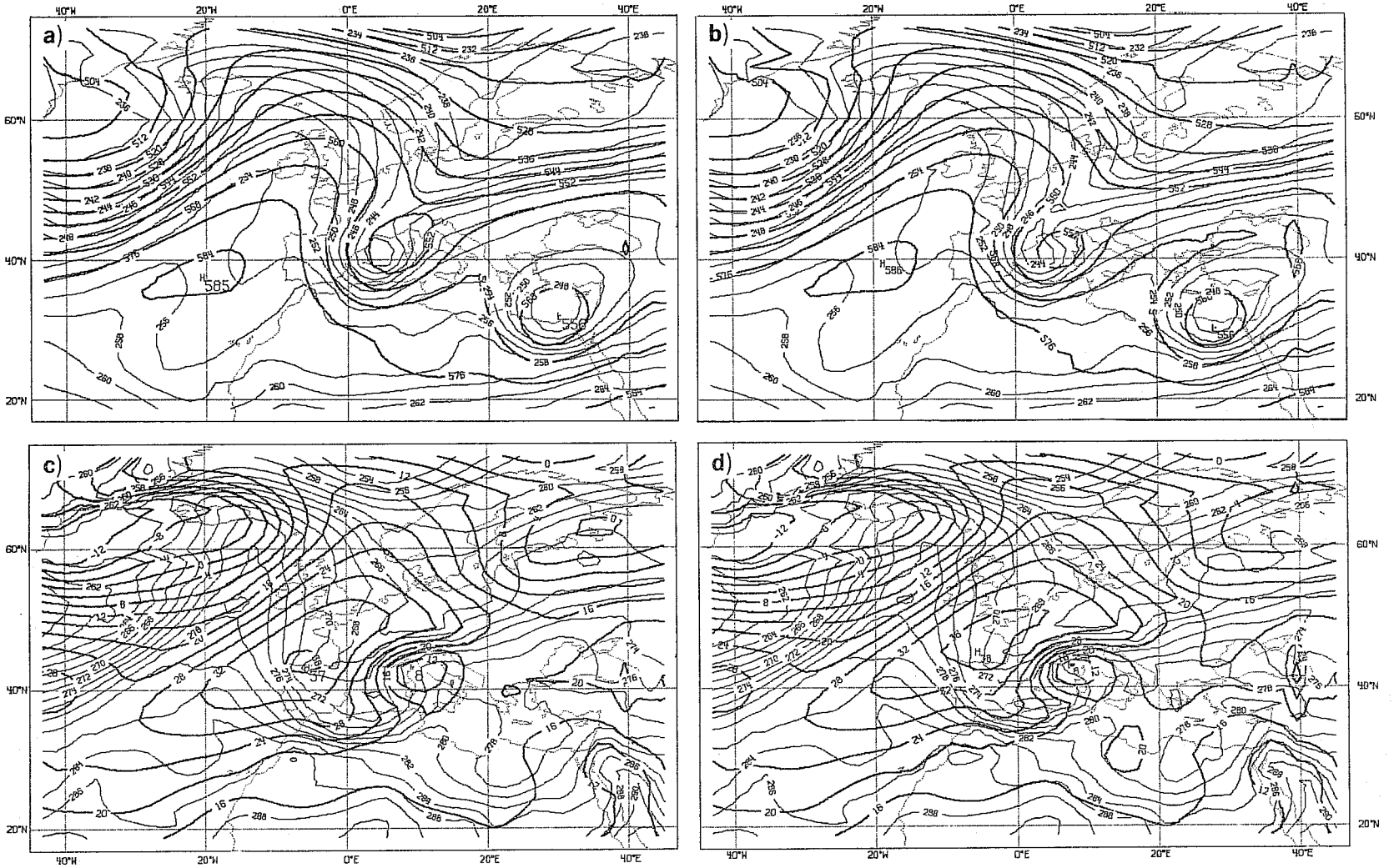

Fig. 23 Maps of the 48 hour forecast from the limited area at N48 resolution with envelope orography with one variance (left), experiment D, and two variances (right), experiment E. Top and bottom respectively as a) and b) in Fig. 6.

Verification time 12 GMT 5 March.

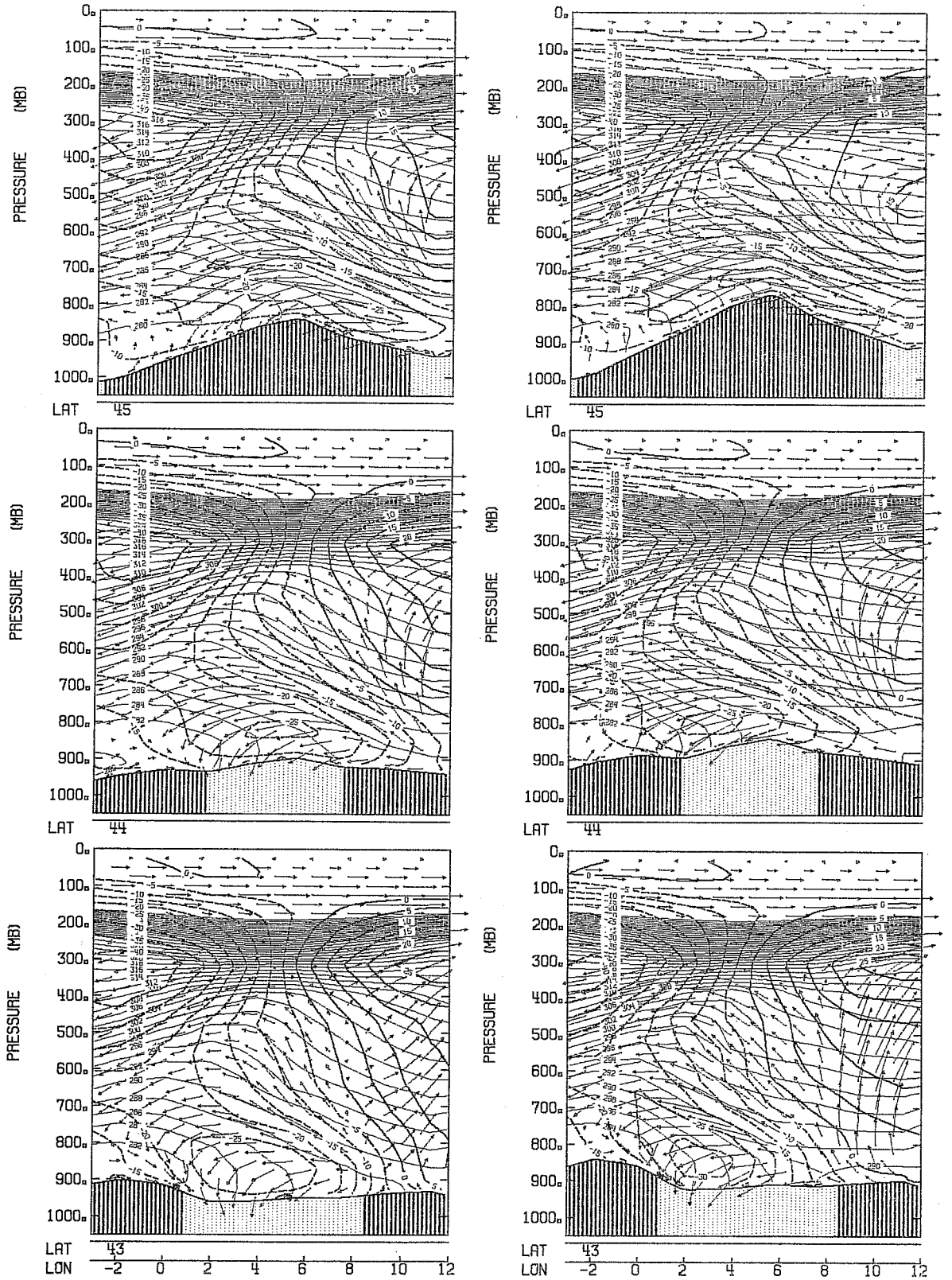

Fig. 24 Vertical cross section from the 48 hour limited area model forecast at N48 resolution with envelope orography with one variance (left) and two variances (right), at latitudes and longitudes described in the figure. (Units as in Fig. 14).

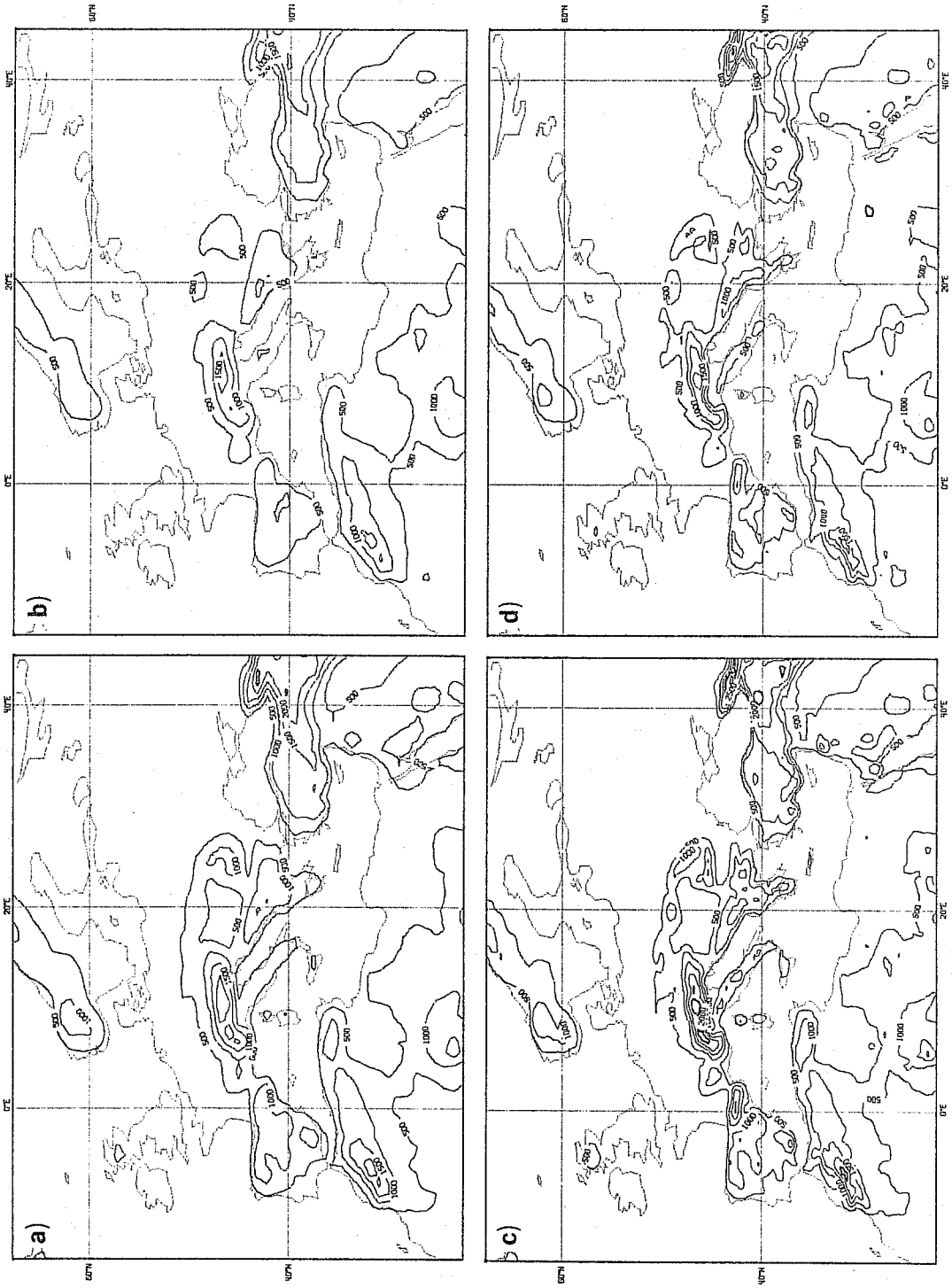

Fig. 25 Maps of the envelope orography with one variance (left) and average orography (right), at resolution N96 (top) and N192 (bottom).

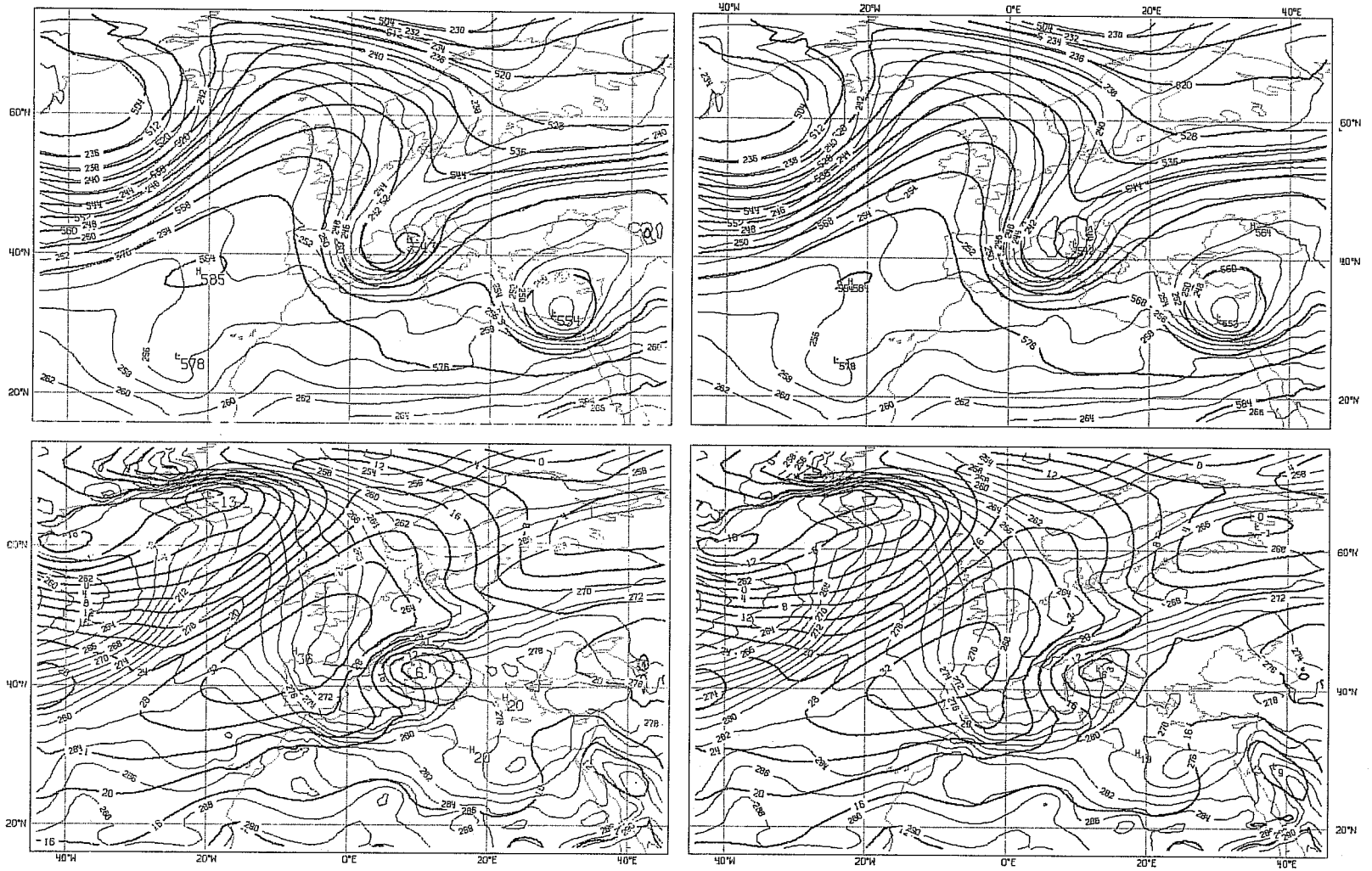

Fig. 26 Maps of the 48 hour limited area model forecast at resolution N96 with envelope orography with one variance (left), experiment F, and average orography (right), experiment G. Top and bottom as in Fig. 6.

Verification time 12 GMT 5 March.

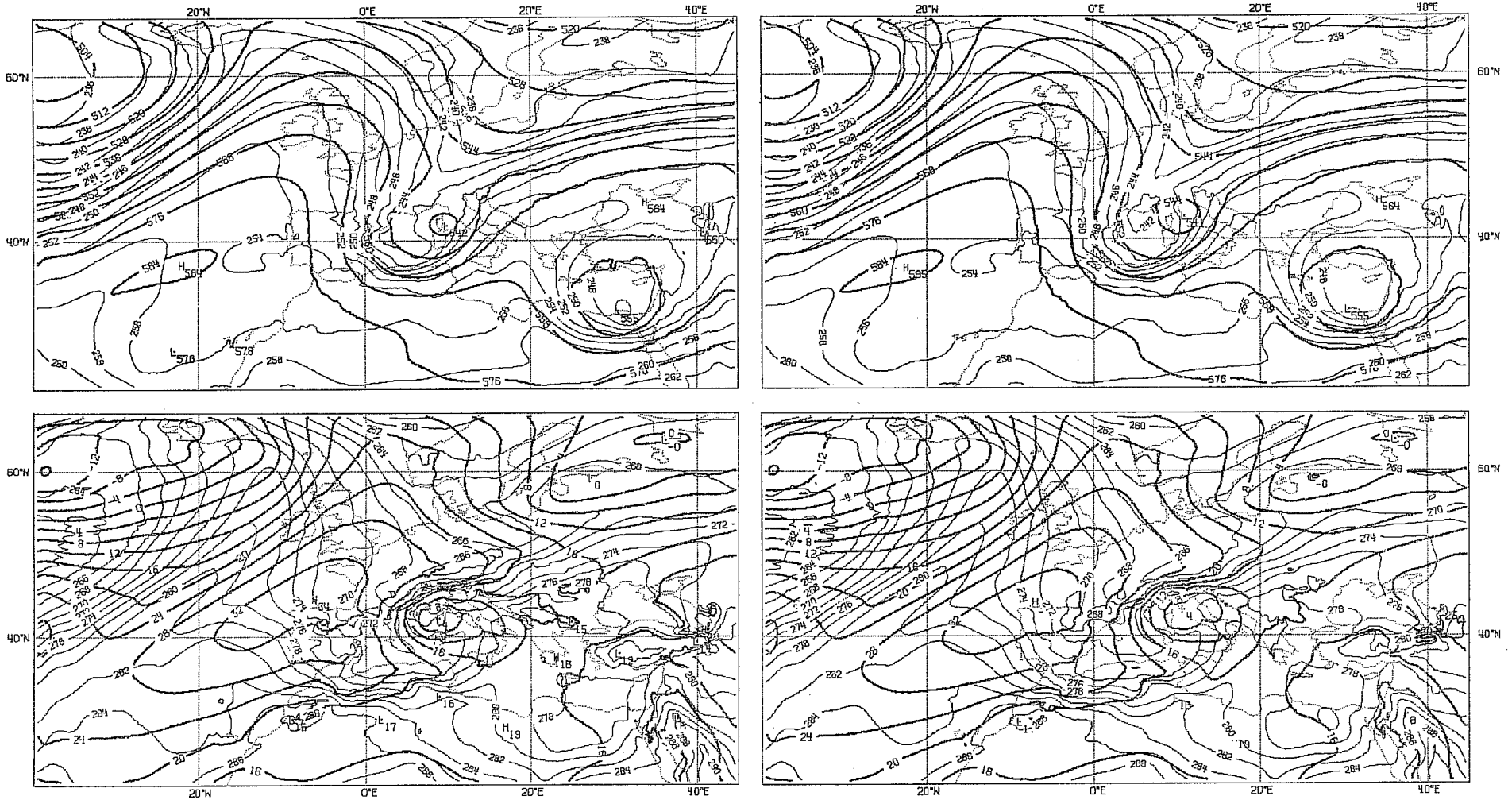

Fig. 27 Same as Fig. 26 for the N192 resolution, experiment H (left), experiment I (right).
Verification time 12 GMT 5 March.

Figs.25c and d show the '1σ envelope' and 'average' orographies at N192 resolution. The former is evidently higher and bulkier than the latter and this is reflected in the forecast. Experiments H and I (see Fig.27) both have resolution N192 - the former with the '1σ envelope' orography and the latter with the 'average' orography. The geopotential height at 500 mb of experiment H, even though it still contains the errors seen in experiment E, shows a cut-off low better positioned than in the previous experiments and even better than in experiment I. Also the axis of the trough is less tilted than in experiment E and the shape is more similar to that one of the analysis. However the field of temperature shows some distortions which are due to the presence of a particularly steep orography that affects, even if only slightly, the field of geopotential. At 1000 mb, experiment I is obviously best. The centre of the cyclone is near the coast of Italy and not west of Corsica (as in experiment H) and quite a few of the features that are apparent in the subjective analysis are present. The cyclone has a double structure with its depth is as observed; all the ridge upwind and the trough in the lee of Pyrenees, Atlas, Appennines and Dinaric Alps are present.

SUMMARY AND CONCLUSIONS

This article describes the results from the case study of cyclogenesis that occurred during the ALPEX period. Recent results obtained from similar experiments allow us to draw some general conclusions.

A preliminary comparison is made between an objective analysis (operational at ECMWF) and a subjective analysis drawn with the intention of preserving all the mesoscale features contained in the observations. From this comparison it is evident that many details are not represented by the objective analysis. Hence there is a need for a much more refined analysis, both to provide the initial data for high resolution models and to verify the results of those models in their detail.

The N48 resolution forecast from the global grid point model and the LAM appear to be very similar, but they are inadequate in their simulation of the cyclogenesis, both because of the low resolution and smooth orography. The N192 resolution forecast with the LAM is capable of a very accurate and detailed weather forecast; being able to reproduce the position, shape and depth of the cyclone, the strength and direction of the wind, the detail of the precipitation and the local effects of the orography. The orography that gives the best results at N192 resolution is the 'average' type. This is derived from the US Navy orography which has a resolution more similar to that of the model.

The result of using the horizontal resolution with very smooth mountains demonstrates that by increasing the resolution of the model, the short-scale features of the circulation, such as small eddies, are taken into account; the model also becomes more responsive to changes in albedo, land-sea contrast and orography (even if smooth). The need for an appropriate orographic representation is clearly demonstrated; an inadequate prescription of orography being responsible for the inaccurate positioning and strength of systems over land. The use of the 'envelope' orography is an effective method for the parameterization of sub-grid-scale mountain forcing. The requirement for an envelope-like parameterization decreases with increasing resolution since the multiple (e) of the standard deviation to be added to the grid-square mean orography appears to be inversely proportional to the resolution.

Further studies are needed on the physical processes represented in the model, mainly in relation to the precipitation. Also further experiments are necessary to provide a better statistical basis for the conclusions presented above. Neverthless, it seems possible to conclude that a more accurate forecast can be obtained using high resolution models that are able to resolve mesoscale systems, which are important for the local weather, but are often misrepresented and even missed by the present general circulation models.

ACKNOWLEDGEMENTS

I am indebted to all those who previously worked in building and developing the limited area model and in particular to D.Burridge and J.-F.Louis. I am grateful to J.Haseler for helping me in the interpolation problems, to S.Tibaldi for useful suggestions on the orography and to M.Brunetti of the Italian Meteorological Service for providing me with a fine hand-drawn analysis.

REFERENCES

Anthes, R.A., Y-H. Kuo, S.G. Benjamin and J-F.Li, 1982: The evolution of the mesoscale environment of severe local storms: preliminary modelling results. Mon.Wea.Rev. 110, 1187-1213.

Anthes, R.A. and D.Keyser, 1979: Test of a fine mesh model over Europe and the United States. Mon.Wea.Rev., 106, 1045-1078.

Burridge, D.M. and Haseler, J, 1977: A model for medium range weather forecasts - adiabatic formulation. ECMWF Tech.Rep.No.4, 46pp.

Davies, H.C., 1976: A lateral boundary formulation for multi level prediction models. Quart.J.R.Met.Soc., 102, 405-518.

Estoque, M.A., 1961: A theoretical investigation of the sea breeze. Quart.J.Roy.Met.Soc., 87, 136-146.

Klemp, J.B. and D.K. Lilly, 1978: Numerical simulation of hydrostatic mountain waves. J.Atmos.Sci., 35, 78-107.

Mahrer, Y. and R.A.Pielke, 1976 Numerical simulation of air flow over Barbados. Mon.Wea.Rev., 104, 1322-1402.

Tibaldi, S., 1980: Cyclogenesis in the lee orography and its numerical modelling, with special reference to the Alps. Chapter 7, orographic effects in planetary flow. Editors R.Hide and P.White. GARP Publication series No.23, WMO, Geneva.

Tiedtke, M., J-F. Geleyn, A.Hollingsworth, J-F. Louis, 1979: ECMWF model, parameterization of subgrid scale processes. ECMWF Tech.Rep.No.10, 46pp.

Trevisan, A., 1976: Numerical experiments on the influence of orography on cyclone formation with an isentropic primitive equation model. J.Atmos.Sci., 33, 768-780.

Wallace, J.M., S.Tibaldi and A.J.Simmons, 1983: Reduction of systematic forecast errors in the ECMWF model trough the introduction of an envelope orography. Quart.J.Roy.Met.Soc., 109, October Issue (in print).

APPENDIX - THE LIMITED AREA MODEL

In Table A a description of the ECMWF grid-point model is given, which is appropriate for the limited area model. The LAM can be used over any region of the globe (except the poles). It has relaxation boundary conditions of the Davies type, Davies (1976), as implemented by Kallberg (private communication) and a maximum resolution of ~46° in both north-south and west-east direction. At present the initial data is obtained from the global objective analysis at N48 resolution. An interpolation is needed when resolutions higher than N48 are used. This is done by fitting the global data with spherical harmonics. The boundary values are updated every time step by using linearly interpolated data taken from the analysis or the global forecast every 12 hours. The inclusion of orographies different from that one used operationally at ECMWF raises the problem of initialization. Interpolation procedures for limited area models are at present in a very early stage. Our practise (Mahrer et al 1976) has been to allow the difference of height between new and old orography to grow in the first 12 hours of the forecast with appropriate changes being made to the surface pressure to conserve mass.

Table A

ECMWF - GLOBAL FORECASTING SYSTEM, 15-level grid point model

(Horizontal Resolution 1.875° Lat/Lon)

ANALYSIS	PREDICTION
ϕ,u,v,q(for p≥300)	T,u,v,q
p(mb)	σ
10	0.025(σ_1)
20	0.077
30	0.132
50	0.193
70	0.260
100	0.334
150	0.415
200	0.500
250	0.589
300	0.678
400	0.765
500	0.845
700	0.914
850	0.967
1000	0.996(σ_{15})

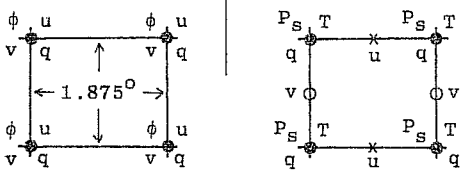

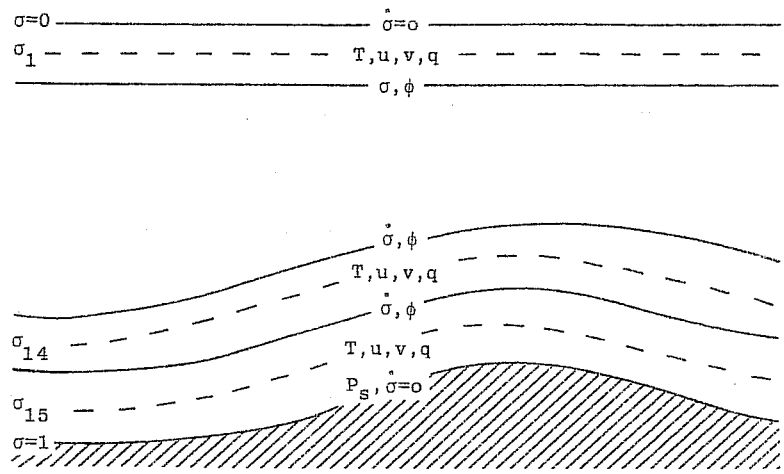

Vertical and horizontal (latitude-longitude) grids and dispositions of variables in the analysis (left) and prediction (right) coordinate systems.

ANALYSIS

Method	3 dimensional multi-variate, correction method for q
Independent variables	λ, φ, p, t
Dependent variables	ϕ, u, v, q
Grid	Non-staggered, standard pressure levels
First guess	6 hour forecast (complete prediction model)
Data assimilation frequency	6 hour ($\pm$ 3 hour window)

INITIALISATION

Method	Non-linear normal mode, 5 vertical modes, adiabatic

PREDICTION

Independent variables	λ, φ, σ, t
Dependent variables	T, u, v, q, p_s
Grid	Staggered in the horizontal (Arakawa C-grid). Uniform horizontal (regular lat/long; $\Delta\lambda=\Delta\theta=1.875^o$). Non-uniform vertical spacing of levels (see above).
Finite difference scheme	Second order accuracy
Time-integration	Leapfrog, semi-implicit (Δt = 15 min) (time filter ν = 0.05)
Horizontal diffusion	Linear, fourth order (diffusion coefficient = $4.5 \cdot 10^{15} m^4 s^{-1}$)
Earth surface	Albedo, roughness, soil moisture, snow and ice specified geographically. Albedo, soil moisture and snow time dependent.
Orography	Averaged from high resolution (10') data set
Physical parameterisation	(i) Boundary eddy fluxes dependent on roughness length and local stability (Monin-Obukov)
	(ii) Free-atmosphere turbulent fluxes dependent on mixing length and Richardson number
	(iii) Kuo convection scheme
	(iv) Full interaction between radiation and clouds
	(v) Full hydrological cycle
	(vi) Computed land temperature, no diurnal cycle
	(vii) Observed sea-surface temperature

ECMWF PUBLISHED TECHNICAL REPORTS

No. 1 A Case Study of a Ten Day Prediction

No. 2 The Effect of Arithmetic Precisions on some Meteorological Integrations

No. 3 Mixed-Radix Fast Fourier Transforms without Reordering

No. 4 A Model for Medium-Range Weather Forecasting - Adiabatic Formulation

No. 5 A Study of some Parameterizations of Sub-Grid Processes in a Baroclinic Wave in a Two-Dimensional Model

No. 6 The ECMWF Analysis and Data Assimilation Scheme - Analysis of Mass and Wind Fields

No. 7 A Ten Day High Resolution Non-Adiabatic Spectral Integration: A Comparative Study

No. 8 On the Asymptotic Behaviour of Simple Stochastic-Dynamic Systems

No. 9 On Balance Requirements as Initial Conditions

No.10 ECMWF Model - Parameterization of Sub-Grid Processes

No.11 Normal Mode Initialization for a multi-level Gridpoint Model

No.12 Data Assimilation Experiments

No.13 Comparison of Medium Range Forecasts made with two Parameterization Schemes

No.14 On Initial Conditions for Non-Hydrostatic Models

No.15 Adiabatic Formulation and Organization of ECMWF's Spectral Model

No.16 Model Studies of a Developing Boundary Layer over the Ocean

No.17 The Response of a Global Barotropic Model to Forcing by Large-Scale Orography

No.18 Confidence Limits for Verification and Energetics Studies

No.19 A Low Order Barotropic Model on the Sphere with the Orographic and Newtonian Forcing

No.20 A Review of the Normal Mode Initialization Method

No.21 The Adjoint Equation Technique Applied to Meteorological Problems

No.22 The Use of Empirical Methods for Mesoscale Pressure Forecasts

No.23 Comparison of Medium Range Forecasts made with Models using Spectral or Finite Difference Techniques in the Horizontal

No.24 On the Average Errors of an Ensemble of Forecasts

No.25 On the Atmospheric Factors Affecting the Levantine Sea

No.26 Tropical Influences on Stationary Wave Motion in Middle and High Latitudes

ECMWF PUBLISHED TECHNICAL REPORTS

No.27 The Energy Budgets in North America, North Atlantic and Europe Based on ECMWF Analyses and Forecasts

No.28 An Energy and Angular-Momentum Conserving Vertical Finite-Difference Scheme, Hybrid Coordinates, and Medium-Range Weather Prediction

No.29 Orographic Influences on Mediterranean Lee Cyclogenesis and European Blocking in a Global Numerical Model

No.30 Review and Re-assessment of ECNET - a private network with Open Architecture

No.31 An Investigation of the Impact at Middle and High Latitudes of Tropical Forecast Errors

No.32 Short and Medium Range Forecast Differences Between a Spectral and Grid Point Model. An Extensive Quasi-Operational Comparison

No.33 Numerical Simulations of a Case of Blocking: The Effects of Orography and Land-Sea Contrast

No.34 The Impact of Cloud Track Wind Data on Global Analyses and Medium Range Forecasts

No.35 Energy Budget Calculations at ECMWF: Part I: Analyses

No.36 Operational Verification of ECMWF Forecast Fields and Results for 1980-1981

No.37 High Resolution Experiments with the ECMWF Model: A Case Study